GAS CONDENSATE DAMAGE IN HYDRAULICALLY FRACTURED WELLS

A Thesis

by

ADEDEJI AYOOLA ADEYEYE

Submitted to the Office of Graduate Studies of
Texas A&M University
in partial fulfillment of the requirements for the degree of

MASTER OF SCIENCE

December 2003

Major Subject: Petroleum Engineering

GAS CONDENSATE DAMAGE IN HYDRAULICALLY FRACTURED WELLS

A Thesis

by

ADEDEJI AYOOLA ADEYEYE

Submitted to Texas A&M University
in partial fulfillment of the requirements
for the degree of

MASTER OF SCIENCE

Approved as to style and content by:

Robert A. Wattenbarger (Chair of Committee)	J. Bryan Maggard (Co-Chair of Committee)
Wayne M. Ahr (Member)	Hans C. Juvkam-Wold (Head of Department)

December 2003

Major Subject: Petroleum Engineering

ABSTRACT

Gas Condensate Damage in Hydraulically Fractured Wells. (December 2003)

Adedeji Ayoola Adeyeye, B.S., University of Lagos

Co-Chairs of Advisory Committee: Dr. Robert A. Wattenbarger
Dr. J. Bryan Maggard

This project is a research into the effect of gas condensate damage in hydraulically fractured wells. It is the result of a problem encountered in producing a low permeability formation from a well in South Texas owned by the El Paso Production Company. The well was producing a gas condensate reservoir and questions were raised about how much drop in flowing bottomhole pressure below dewpoint would be appropriate. Condensate damage in the hydraulic fracture was expected to be of significant effect.

Previous attempts to answer these questions have been from the perspective of a radial model. Condensate builds up in the reservoir as the reservoir pressure drops below the dewpoint pressure. As a result, the gas moving to the wellbore becomes leaner. With respect to the study by El-Banbi and McCain, the gas production rate may stabilize, or possibly increase, after the period of initial decline. This is controlled primarily by the condensate saturation near the wellbore. This current work has a totally different approach. The effects of reservoir depletion are minimized by introduction of an injector well with fluid composition the same as the original reservoir fluid. It also assumes an infinite conductivity hydraulic fracture and uses a linear model.

During the research, gas condensate simulations were performed using a commercial simulator (CMG). The results of this research are a step forward in helping to improve the management of gas condensate reservoirs by understanding the mechanics of liquid build-up. It also provides methodology for quantifying the condensate damage that impairs linear flow of gas into the hydraulic fracture.

DEDICATION

I wish to dedicate my thesis:

to the almighty God, I praise you with all my heart,

to Jesus Christ my Lord and Savior,

I thank you for being so good to me;

to my parents, uncle, cousins, brothers, sister, friends and sweetheart for their motivation, help, and support. I love you all.

ACKNOWLEDGEMENTS

I wish to express my sincere gratitude and appreciation to Dr. Robert A. Wattenbarger, co-chair of my advisory committee, for his continued help and support throughout my research. He is a great mentor and I am grateful for the opportunity to be one of his students.

I wish to express my sincere gratitude and appreciation to Dr. J. Bryan Maggard, co-chair of my advisory committee, for his active participation and guidance during my investigation. My simulation results would never have been perfect without him. My thanks also go to Dr. Wayne Ahr, for his encouragement.

I express my gratitude and appreciation to the Petroleum Engineering Department for financial support in the form of assistantships.

TABLE OF CONTENTS

Page

CHAPTER Page

LIST OF FIGURES

FIGURE Page

LIST OF TABLES

CHAPTER I

INTRODUCTION

1.1 Gas condensate reservoirs

Gas condensate reservoirs are receiving more attention in the petroleum industry because they are becoming more commonplace as hydrocarbon exploration moves to deeper geological strata, including offshore structures. In the North Sea, for instance, gas condensate reservoirs represent a significant part of the total hydrocarbon reserves. These reservoirs are usually encountered at high pressures and temperatures, and the fluid system is found at near-critical conditions.

Wells in gas condensate reservoirs often experience rapid decline when the near wellbore pressure goes below the dewpoint pressure. Radial compositional simulation models were often used to investigate the problem of productivity loss[1-6]. These models clearly show that the loss in productivity was due to liquid drop out near the wellbore. This so-called condensate blocking (increase in condensate saturation around the wellbore) reduces the effective permeability to gas and results in a rapid decline in well productivity once the near wellbore pressure drops below the dewpoint.

The effect of condensate blocking is more evident in low permeability reservoirs. Barnum *et al*[7] showed that the recovery factor of gas condensate radial wells is only affected by condensate blocking if the well's *kh* is less than 1,000 md-ft. For higher quality reservoirs, productivity loss is not very severe.

This thesis follows the style of the *SPE Reservoir Evaluation and Engineering Journal.*

El-Banbi *et al*[8] showed that the well productivity of vertical wells in a moderately rich gas condensate reservoir initially decreased rapidly and then increased as the reservoir was depleted. This phenomenon was explained by compositional simulation. Initially, when the wells go below the dewpoint, the productivity decreases because of the high condensate saturation in the ring (areas around the wellbore), which severely reduces the effective permeability to gas, thereby reducing gas productivity. However, the wells showed approximately stable gas production after the period of an initial decline and a subsequent increase in gas production rate. The gas flowing into the ring became leaner causing the condensate saturation in the ring to decrease. This increased the effective permeability of the gas and caused the gas productivity to increase as was observed in field data. Their work was a tremendous help in understanding the dynamics of condensate build-up around wellbores in gas-condensate fields.

1.2 Use of hydraulic fractures

Over the years, hydraulic fracturing has proven to be one of the most effective techniques for improving the productivity of dry gas reservoirs. Hydraulic fractures are used to overcome formation damage and to increase the conductivity of flow path of fluid to the wellbore. It has also been found to be effective in improving the productivity of gas condensate reservoirs. Kroemer *et al*[9] showed that non-Darcy effects are minimized and the well will suffer less productivity reduction once condensate blocking occurs.

The state of stresses of the formation governs which orientation the fracture will take. Fractures will open in a direction perpendicular to the minimum stress. Normally, vertical fractures will develop for formation depth greater than 2,000 feet and horizontal fractures will develop for shallower formations[10]. Linear flow perpendicular to the fracture will be seen in the early time performance of any fracture configuration if the fracture conductivity is high.

Al-Hashim and Hashmi[11] showed that hydraulic fracturing is effective in improving the productivity index (PI) of gas condensate wells both above and below the dewpoint pressure by about three times as compared to the non-fractured wells. Hydraulic fractures are also found to extend cumulative production above the dew point pressure. As dimensionless fracture conductivity increases, the long-term performance of the gas condensate reservoir is improved, and the improvement is more pronounced for longer fractures. Once the dewpoint is reached, the flowing bottomhole pressure drops sharply to the specified minimum flowing bottomhole pressure in fractured and non-fractured wells. However, the drop is less severe in the fractured case. The sharp drop in the flowing bottomhole pressure, results in reduction in the productivity of gas condensate wells.

Long fractures are warranted for low-permeability reservoirs; wide but short fractures are indicated for high permeability formations.[11-16] Romero *et al*[12] found that the fracture face skin effect had a significant detrimental effect on the dimensionless productivity index, especially for high-permeability reservoirs.

Wang *et al*[13] presented a model that predicts the fractured well performance in gas-condensate reservoirs, quantifying the effects of gas permeability reduction. However, guidelines for the calculation of the appropriate pressure drawdown during production to optimize well performance were not very clear.

1.3 Overview

This work is a result of a problem encountered in producing Smith #1, a well owned by the El Paso Production Company. The well was producing a tight gas condensate reservoir. Questions were raised about how much drop in flowing bottomhole pressure below dewpoint would be appropriate, and the gas condensate damage in the hydraulic fracture was expected to be of significant effect. With all the work done thus far,

previous authors tackled the problem from a radial model perspective. This current work used a linear model to represent an infinite conductivity fractured well, and therefore gives a more appropriate analysis of condensate damage extending from the hydraulic fracture face.

Chapter II of this thesis presents a comprehensive review of the theory and latest investigations regarding hydraulic fracturing, condensate damage, and reservoir fluid characteristics, and how these factors may affect the fluid distribution in the reservoir and the drawdown appropriate for producing wells.

In Chapter III, the results of simulation are compared to analytical solutions for skin in a single-phase system. It goes over rudimentary concepts and does a good job of validating some very important analytical solutions for skin. It also serves to investigate geometry effects, by comparing skin damage in a radial model, which represents the wellbore, to that of a linear model, which is representative of a hydraulic fracture. The chapter helps to quantify fracture face skin and also gives an idea of its relative magnitude of detriment to productivity, compared to skin from the Hawkins' approach.

Chapter IV covers the adaptation of a compositional fluid model in CMG's data file collection, and the construction of the 1-D linear model used in simulation, including the definition of reservoir dimensions and grid-size. The 1-D linear model is quite analogous to the hydraulic fracture, for an infinite conductivity fracture. For the purposes of this research, it is used to investigate the effect of condensate build-up near hydraulic fractures, as the reservoir pressure depletes and near wellbore pressure falls below the dewpoint pressure. The goal is to quantify the damage that results from the condensate build-up and note its effect on pressure drawdown, which eventually translates into gas production. Finally, recommendations for future work are discussed, and conclusions are reached in Chapters V and VI respectively.

CHAPTER II

LITERATURE REVIEW

2.1 Gas condensate reservoir fluid modeling

Gas condensate reservoirs are initially at a pressure above the dewpoint pressure, therefore, the reservoir contains single-phase gas. As production begins gas flows through the porous system, through the production wells, and finally to the separation facilities, where liquids condense from the gas. As reservoir pressure falls below dewpoint, *in-situ* condensation starts, and the liquid formed accumulates in the porous network until it reaches the minimum saturation required to begin moving, which is called the critical condensate saturation (S_{cc}).

Once the condensate saturation reaches S_{cc}, it begins to flow through the porous system towards the producers but it may be also pulled down because of gravitational forces, depending on the vertical communication and the heterogeneity of the porous media.

In reservoir simulation, an equation of state is tuned to represent the thermodynamic behavior of the reservoir fluids as a function of pressure and composition, which vary both with depth and during production.

Metcalfe *et al*[17] used a field sample of gas condensate fluid to run several pressure, volume and temperature (*PVT*) laboratory tests, such as constant composition expansion (*CCE*) and constant volume depletion (*CVD*), to show that the distribution of the heavy-component cuts vary with respect to sampling depth. In addition, they compared the results of the *CCE* obtained using a black-oil model and a compositional model with the experimental results. They observed that black-oil model could predict dewpoints for leaner systems, while the black-oil predictions deviate from the experiments for richer

systems. These results indicate that the proper procedure to model these fluids is by fully compositional simulation.

Creek[18] calibrated the Peng-Robinson equation of state to predict the variation of composition, solution gas-oil ratio, and saturation pressure within a reservoir affected by compositional gradient. He also explained the variation in bubblepoint and dewpoint as a consequence of the differences in composition. He demonstrated that the variation of composition because of the force of gravity is stronger for rich gases.

Fevang *et al*[19] studied a variety of fluids ranging from medium rich gas condensate to near critical fluids using black-oil and compositional models. They simulated production for both injection and natural depletion production schemes and compared the results obtained with both models. They concluded that gas condensate produced by gas cycling above the dewpoint could be simulated accurately with a black-oil simulator. However, they also found for the case of rich gas condensate where permeability increases with depth, that black-oil simulators significantly over-predict oil recovery owing to compositional effects that are not properly treated in a black-oil model. They concluded that the black-oil model consistently over-predicts oil production because oil vaporization is over-estimated.

Fevang *et al*[19] recommended the use of compositional simulation models for gas injection studies and limited the use of black-oil model only for reservoir fluids with minimal vaporization, and lean gas condensate reservoirs undergoing cycling injection above the dewpoint pressure.

2.2 Tight gas reservoirs

As the oil and gas industry matures, ongoing targets move towards more challenging prospects commonly exhibiting low permeability and often low pressure. Considerable effort has been expended in a number of areas in the Deep Basin area in Canada, the powder River Basin in the Central United States and the Permian basin in the Texas area in attempting to exploit gas reservoirs with average permeability in the less than 0.1 md range. For the purpose of this research, the models under investigation will be tight gas reservoirs.

Bennion *et al*[20] discussed the issue associated with the identification of productive, low-permeability gas producing formations and the successful completion and production of these reservoirs. Criteria were presented for identifying economic absolute permeability cutoffs for low permeability gas-bearing formations. Retention of fluids (phase trapping) was presented as one of the major mechanisms of reduced productivity, even in successfully fractured completions in these types of formations. In general, as permeability and porosity are decreased, both the capillary pressure value and the value of the irreducible water saturation tend to increase substantially. Often associated with this increase in trapped initial liquid saturation is a significant reduction in net effective permeability to gas caused by the irreducible and immobile trapped initial liquid present in the porous media. In reservoir situations where exceptionally low permeability were present, the authors found that if the reservoir is in a normally saturated condition (that is, if the reservoir is in free contact and capillary equilibrium with mobile water and is at a normal level of capillary saturation for the specific geometry of the porous media under consideration), very high trapped initial liquid saturations tend to be present. It was observed that in most cases where very low permeability gas reservoirs were potentially productive, the reservoir sediments had been isolated from effective continual contact with a free water source, which was capable of establishing an equilibrium and uniform capillary transition zone. The authors suggested that a combination of long-term regional migration of gas through the isolated sediments (resulting in an extractive desiccating effect as temperature and pore pressure are increased over geologic time), may be

responsible for what they referred to as a "sub-irreducible" initial water saturation condition. This condition is when the reservoir exhibits an average initial water saturation less than the irreducible water saturation expected to be obtained for the porous media at the given column height present in the reservoir above a free water contact (based on a conventional water-gas capillary pressure drainage test). They noted that in situations where exceptionally low matrix permeability is present in a gas-producing reservoir, unless a sub-irreducibly saturated original condition is present, the reservoir would exhibit insufficient initial reserves or effective permeability to be a viable gas-producing candidate.

2.3 Relative permeability

Fluid-flow calculations in reservoir rocks require the use of effective permeabilities which express the rock's ability to flow a specific fluid through a porous medium when more than one phase is present in the pore space. The effective permeability is usually expressed as a ratio of the absolute permeability, which is commonly chosen as the base permeability and this ratio is called the relative permeability. A judicious assignment of the relative permeability model helps ensure that fluid movement in reservoir rocks is reasonably modeled. A reliable representation of the fluid-flow throughout the reservoir is obtained when there is a good match between the simulated and the actual production history.

Relative permeability modeling has been one of the most important topics studied for gas condensate reservoirs over the last decade because of the problems related to direct measurements of relative permeability for these reservoirs.

Some researchers[21] considered two different regions in gas condensate reservoirs based on the flow regime, one near to the producer, and another far from the well in a radial case. This region is usually subdivided into two sectors. Sector *A* is above the dew point pressure, where only gas is flowing through the reservoir. This is characterized by low flow rates and is affected by the gas injection process. The permeability in this sector is evaluated as effective permeability using Darcy's law. Sector *B* occurs where the flow rate is still low but liquid drops out occurs because the system pressure falls below the dewpoint. **Fig. 2.1** illustrates the flow regions in a gas condensate reservoir producing by depletion. Boundaries between sectors and regions are dynamic during the life of the reservoir, and may also not be present, or disappear.

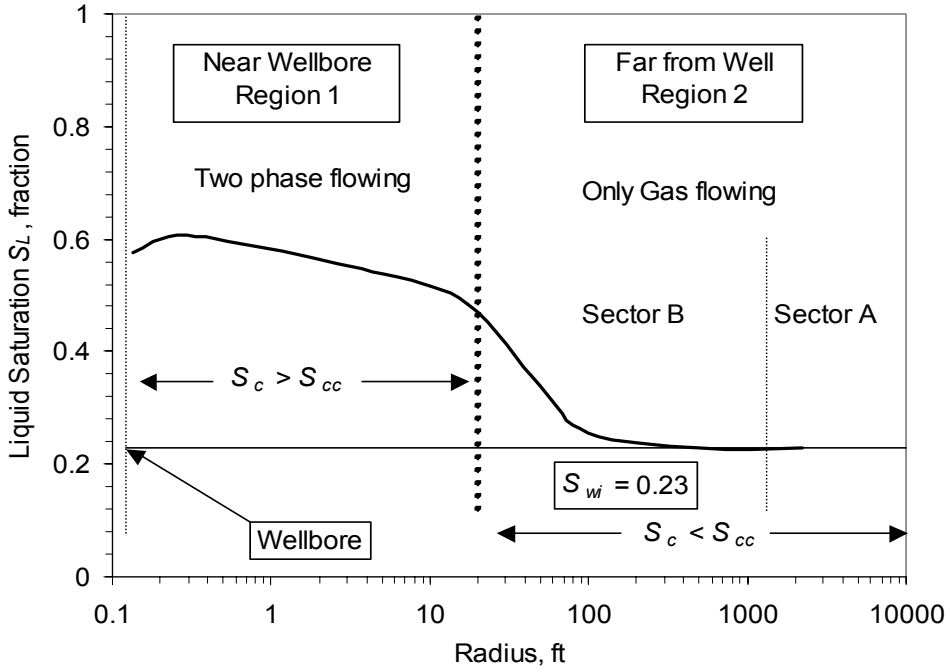

Fig. 2.1 - Flow regions in gas condensate reservoir producing by depletion after Zapata[24]

For the purpose of this research, the effects of reservoir depletion are minimized by introduction of an injection well with fluid composition the same as the original reservoir fluid and bottomhole injection pressure at the initial reservoir pressure. The method of 3-phase relative permeability calculation used is the Stone's method II.

CHAPTER III
PRODUCTION IMPAIRMENT

The concept of skin factor or damage due to skin has been very useful in the quantification of impediment to flow in oil and gas production. The most common is damage around the wellbore, denoted by skin factor, *s*. In the case of hydraulic fractures the analogy to wellbore skin, is the fracture face skin, s_{ff}, which is a permeability reduction normal to the face of the fracture. In this chapter, the results of simulation are compared to analytical solution for skin in a single-phase system. Geometry effects are also investigated, by comparing skin damage in a radial model, which represents the wellbore within a circular drainage area, to that of a linear model, which is representative of an infinite conductivity hydraulic fracture. The simulations are done using GASSIM, a 2-D real gas simulator used for single-phase fluid (liquid or gas).

Well test analysis normally uses a general approach for providing solutions to the diffusivity equation[22]. The general solutions rely on the concepts of dimensionless pressure and dimensionless time.

$$\text{Dimensionless pressure, } p_D = \frac{kh\left(p_i - p_{wf}\right)}{141.2qB\mu} \quad \text{.....(3.1)}$$

$$\text{Dimensionless time, } t_D = \frac{0.00633kt}{\phi\mu c_t r_w^{\,2}} \quad \text{.....(3.2)}$$

$$p_D = \tfrac{1}{2}\ln t_D + 0.4045 + s \quad \text{.....(3.3)}$$

The physical pressure drop in the steadystate radial flow situation is equal to a dimensionless pressure drop, which is equivalent to the skin factor, s.

$$\text{Skin factor, } s = \frac{kh\Delta p_s}{141.2qB\mu} \quad \text{.....(3.4)}$$

The same concept applies to transient flow and to more complex situations – only the dimensionless pressure function is different. It is this generality that makes the dimensionless-solution approach useful.

3.1 Wellbore skin effects

This section uses a simple radial model to illustrate the comparison of simulation results to the Hawkins' approach. The synthetic reservoir used in simulation has 3,000 ft drainage radius with an initial pressure of 3,000 psi, porosity equal to 0.23, and permeability equal to 0.1 md (See Appendix A for data file). There are 20 grids in the *x*-direction and the permeabilities of the first three grids close to the wellbore are reduced to 0.02 md as shown in **Fig. 3.1**.

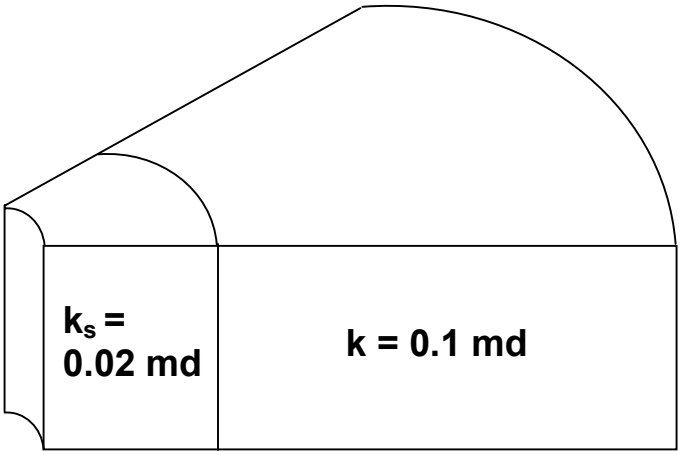

Fig. 3.1 – Permeability reduction close to the wellbore in a radial model

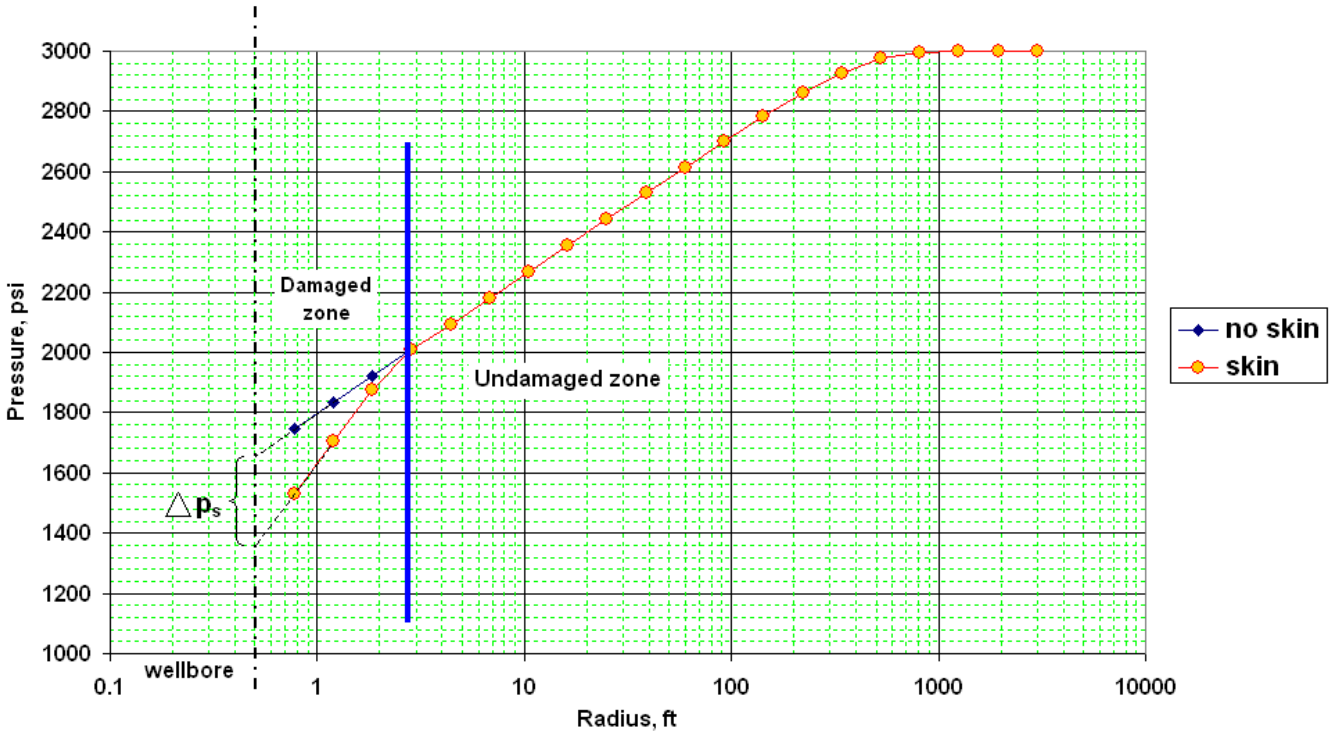

Fig. 3.2 – Radial model pressure profile schematic

The schematic in **Fig. 3.2** shows that a plot of flowing bottomhole pressure against logarithm of radius gives a straight line for a reservoir with no damaged zone. For parts of the reservoir near the wellbore, where the permeability has been reduced, there is a change in the slope of the line. Due to reduced permeability, the slope of the line in the damaged zone is steeper than that in the undamaged zone. The pressure drop due to skin, Δp_s is the term substituted into dimensionless variables and used to compute skin factor.

Fig. 3.3 shows a different approach to analyzing the simulation results. It is a plot of flowing bottonhole pressure against logarithm of time, and it shows that at infinite acting state, simulation runs for both the damaged and undamaged cases have parallel straight lines, which differ by the pressure drop due to skin. In the case of damage, for time less than 0.1 days, the slope of the line is steeper due to the effects of transient flow.

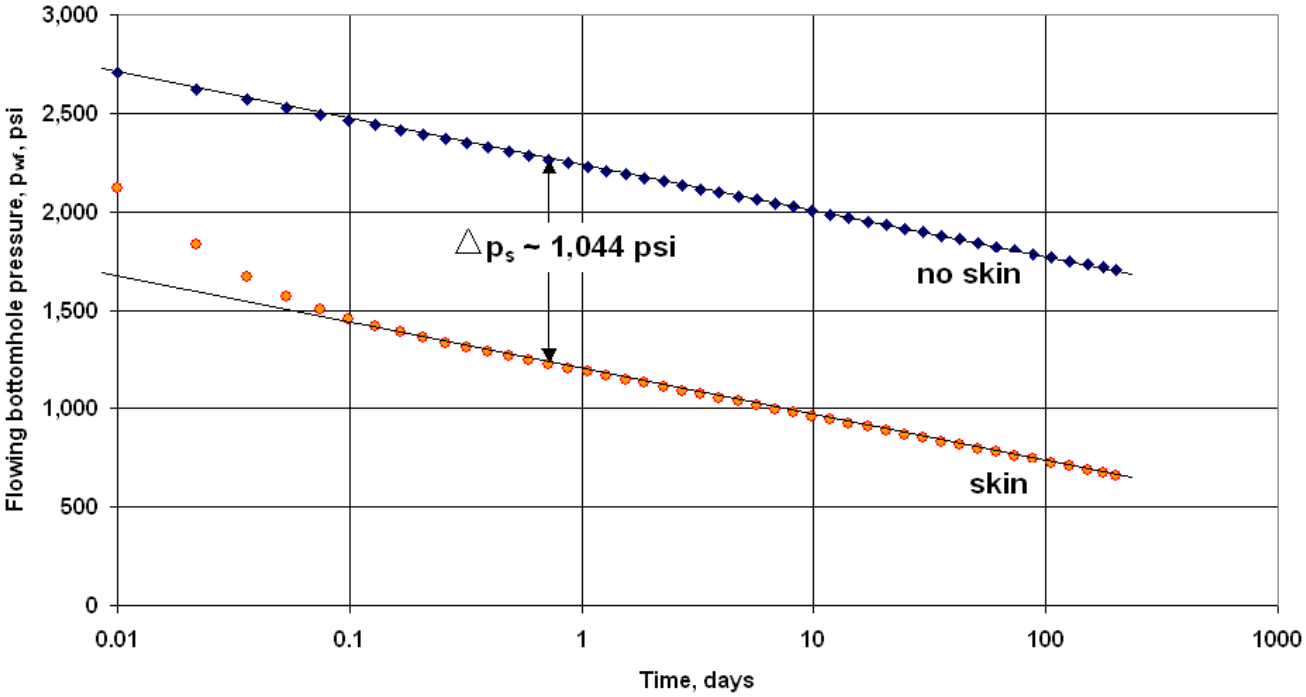

Fig. 3.3 – Pressure drop due to skin in the radial model simulation

From Fig 3.3, $\Delta p_s = 1{,}044$ psi.

$$\text{Recall, skin factor, } s = \frac{kh\Delta p_s}{141.2qB\mu} \quad \text{.....(3.4)}$$

Substituting for q, the constant rate; k, h, μ, and B, the reservoir properties. The skin factor is 5.22 (dimensionless).

From Hawkins' equation,

$$\text{Skin factor, } s = \left(\frac{k}{k_s} - 1\right)\ln\frac{r_s}{r_w} \quad \text{.....(3.5)}$$

where, reservoir permeability, k = 0.1 md; damaged zone permeability, k_s = 0.02 md; wellbore radius, r_w = 0.5 ft; and damage extent, r_s = 1.844 ft.

Upon substitution, the skin factor calculated using the Hawkins' formula was equal to 5.22, which was the same as that obtained using the simulation results.

3.2 Fracture face skin

Most wells drilled in low permeability formations need hydraulic fracturing to be able to produce with economic viability. With continued production, there is a permeability reduction normal to the face of the fracture, shown in **Fig. 3.4**, and there is a need for this skin to be quantified. For single-phase fluid, skin effects on the face of a fracture are simulated, and the fracture face skin formula is validated.

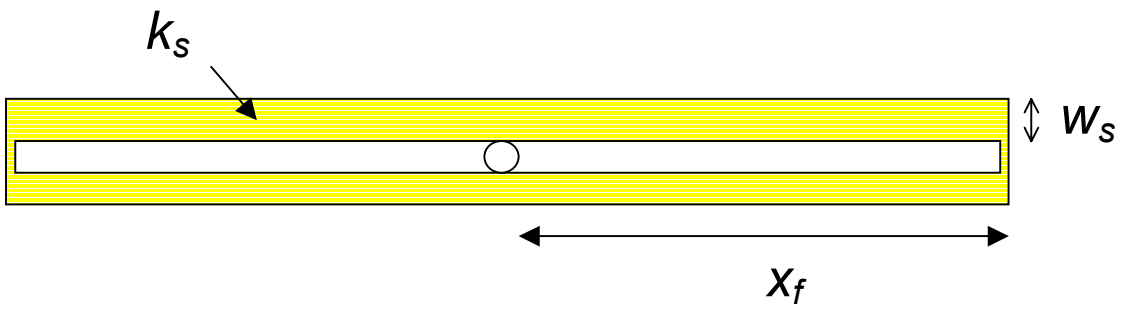

Fig. 3.4 – Permeability reduction normal to fracture face

The case study is an 80-acre tight gas reservoir with reservoir properties given in the data file in Appendix B. For analysis, one-quarter of the reservoir was modeled. The grid set-up for the simulation is illustrated in **Fig. 3.5**.

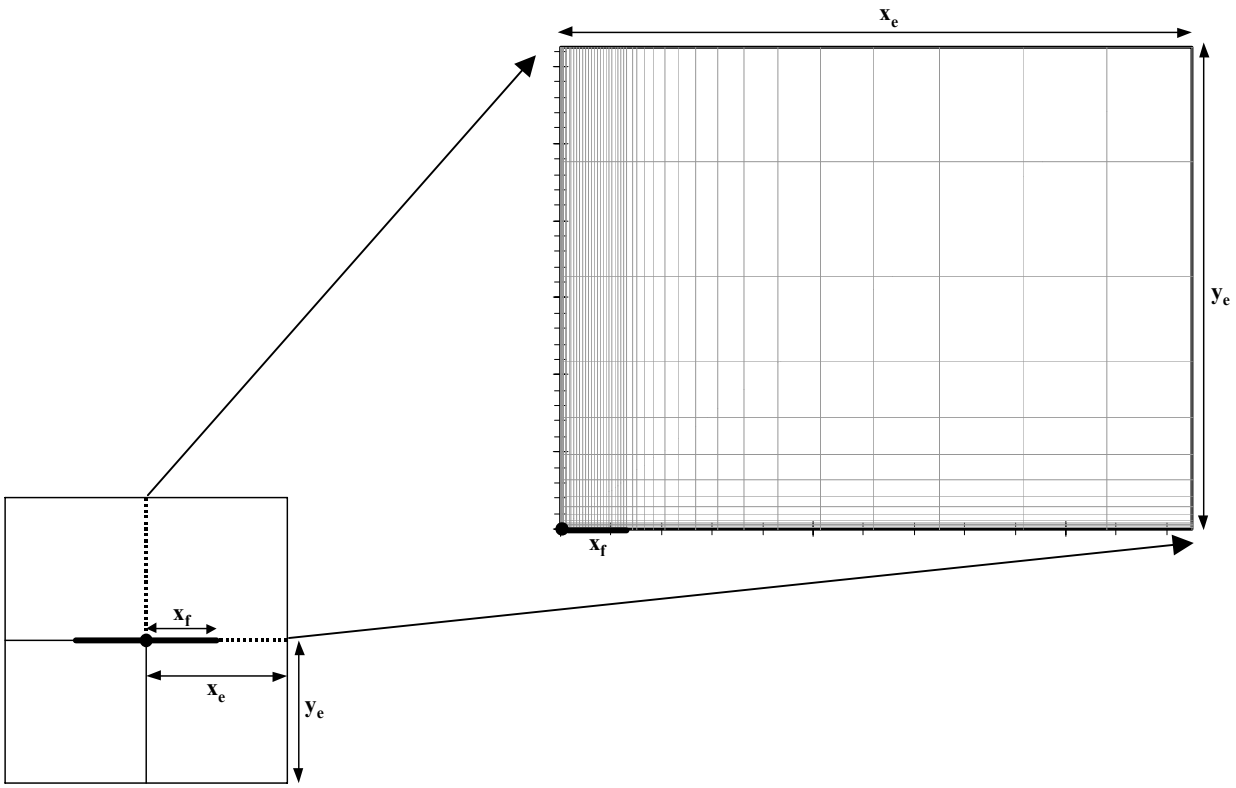

Fig. 3.5 - Quarter model for 80 acre drainage area

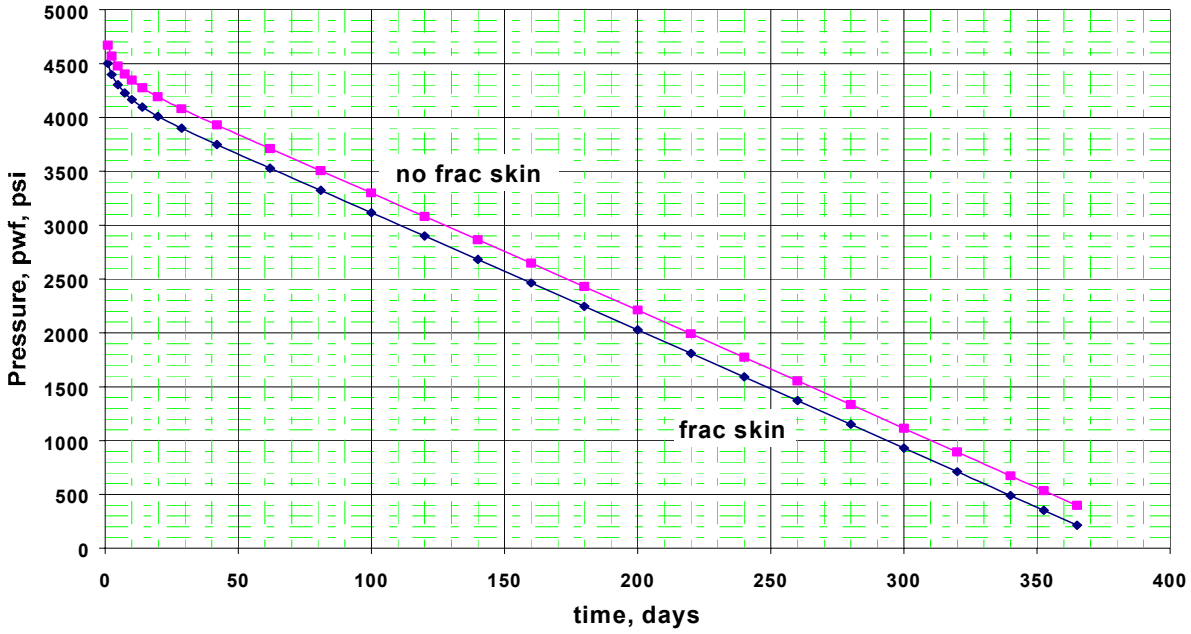

Fig. 3.6 – Fracture face skin effect on flowing bottomhole pressure ($x_e/x_f = 1$)

Assuming an infinite conductivity fracture, the Δp_s is approximately 200 psi and this is equivalent to a fracture face skin value of 0.235. Simulation result for the skin effect in the hydraulic models was matched with the fracture face skin formula validated in Appendix C.

$$\text{Fracture face skin, } s_{ff} = \frac{\pi w_s}{2x_f}\left(\frac{k}{k_s} - 1\right) \quad \text{.....(3.6)}$$

On substitution for the variables, the fracture face skin was computed to be within 98% accuracy, and thus, the formula was validated with simulation results.

3.3 Geometry effects

This section of the chapter is basically a wellbore skin factor and fracture face skin comparison. Its aim is to show the effects of geometry on skin.

Recall the Hawkins' equation,

$$\text{Wellbore skin, } s = \left(\frac{k}{k_s} - 1\right)\ln\frac{r_s}{r_w} \quad \text{.....(3.5)}$$

Assuming $\frac{k}{k_s}$ ratio of 10, and damage extent, r_s of 1 ft

With wellbore radius, r_w = 0.25 ft

$$s = (10-1)\ln\frac{1}{0.25}$$

Skin, s = 12.48 (dimensionless)

Also recall the fracture face skin formula from Appendix C,

$$s_{ff} = \frac{\pi w_s}{2x_f}\left(\frac{k}{k_s} - 1\right) \quad \text{.....(3.6)}$$

Considering similar properties like in the Hawkins' equation example,
With fracture half-length, x_f assumed as 200 ft,

$$s_{ff} = \frac{3.142(1)}{2(200)}(10 - 1) \quad \text{.....(3.7)}$$

s_{ff} = 0.07 (dimensionless)

Comparing skin, s and s_{ff},

$$\frac{s}{s_{ff}} = 178 \quad \text{.....(3.8)}$$

For similar properties used in both equations, the comparison shows that the skin effects at the wellbore are more predominant than skin on the face of the fracture, for typical fracture half-lengths of about 200 ft. With fracture half-length in the field ranging from 100 ft to several hundred ft, half-length contribution to fracture face skin is not insignificant. The longer the fracture half-length, the greater the ratio of wellbore skin factor compared to the fracture face skin.

The results shown in here, only apply to a single-phase fluid system (liquid or gas). In Chapter IV, similar analysis is done for skin, but instead of a single-phase fluid, the model is a compositional fluid system, and the problem becomes a little more complicated.

CHAPTER IV
SIMULATION OF CONDENSATE DAMAGE

In Chapter III, analysis for skin was done considering single-phase fluid (liquid or gas). In this chapter, similar analysis is made but with a rich gas condensate fluid. Due to the accumulation of liquid at pressures below the dewpoint, the quantification of damage in this case becomes quite complex. For simplicity, dimensionless pseudopressure, m_D is introduced and used to develop the relation for skin due to liquid build-up. This project is different from previous work discussed in Chapter III, because its focus is on condensate damage, and the effects of transient and depletion are minimized by introduction of an injector well with fluid composition the same as the original reservoir fluid. The compositional simulation is done using CMG. **Fig. 4.1** gives an overview of condensate build-up process during simulation. The details of the illustration are expanded upon later in the chapter.

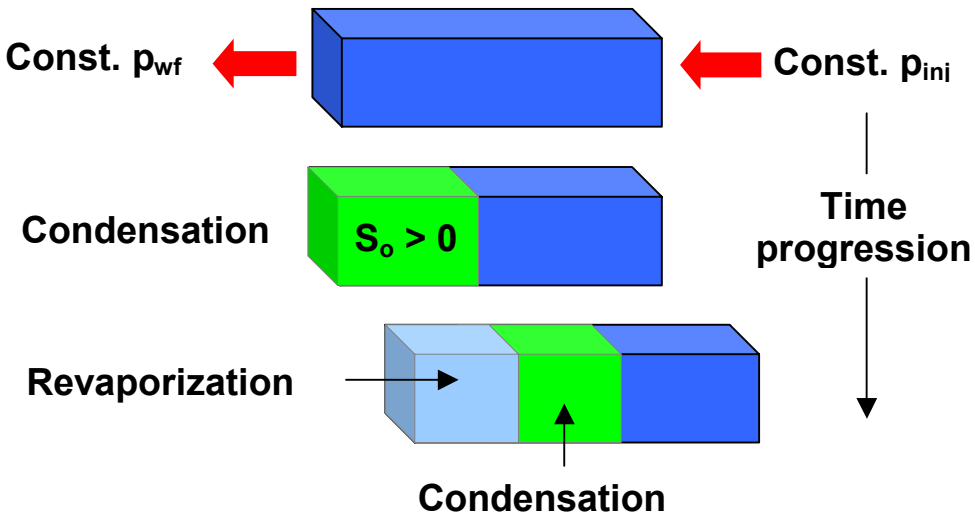

Fig. 4.1 – Schematic of the condensate build-up

4.1 Reservoir description

The reservoir characteristics of CMG's rendition of the third SPE Comparative Solution Project[23] were used to develop a linear model for simulation. The linear model is analogous to linear flow toward an infinite conductivity fracture propagating to the entire extent of the rectangular reservoir. **Table 4.1** summarizes the fundamental characteristics of the reservoir.

Table 4.1 - Main characteristics of the reservoir model

Reservoir Characteristic	**Values**
Drainage Area, Acres	~ 80
Reservoir Half Length (x_e), ft	933
Reservoir Half Length (y_e), ft	933
Thickness (h), ft	50
Absolute permeability (k), md	0.15
Porosity (ϕ), fraction	0.1
Water Saturation (S_w), fraction	0.16
Initial Pressure (p_i), psi	3,900
Injection Pressure (p_{inj}), psi	3,910
Dewpoint Pressure (p_d), psi	3,500
Temperature (T), ^{o}F	200
Total Compressibility (c_g), psi^{-1}	4.0E-06

According to the information presented in Tables 4.1, the dimensions of the linear model are 933 ft in the x and y directions and 50 ft in z direction. These dimensions along with an average porosity of 10% represent the initial gas reservoir volume in the symmetric

quarter of an 80 acres drainage area (**Fig. 3.5)**. The model was divided into 40 grid blocks, 40 in the *x* direction, 1 in the *y* direction, and 1 in the *z* direction.

This reservoir was subjected to gas pressure maintenance using injection fluid of initial reservoir composition. Hence, our model includes both a production well and a gas injector well. These wells were located in the extremes of the linear model as shown in **Fig. 4.2**. Because the main objectives of this research are to understand the mechanics of liquid build-up and specify appropriate pressure drawdown, wells completions were not considered as a primary issue and the wells were completed in the whole interval. It means the both producer and injector wells are open from top to bottom. Also the water saturation was set as 0.16 through the entire model.

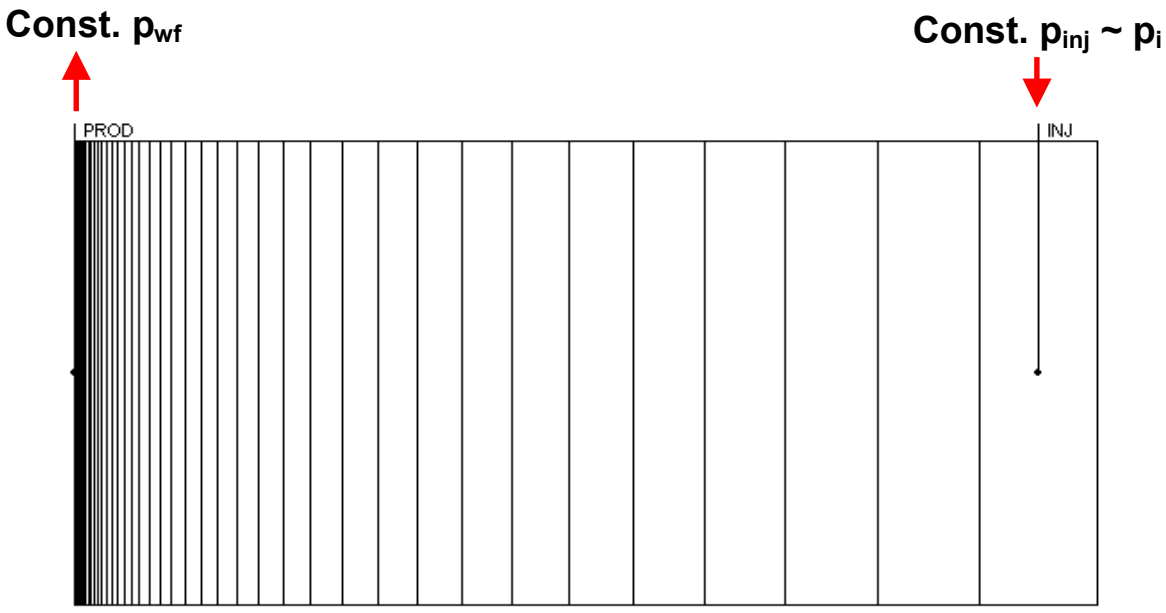

Fig. 4.2 – Case study: 1-D linear model

Once all required information regarding the dimensions of the reservoir model were established, a synthetic simulation model was created using CMG version 2002.10. The base saturation-relative permeability tables used were those reported in the data file adopted from CMG sample data related to third SPE Comparative Solution Project[23].

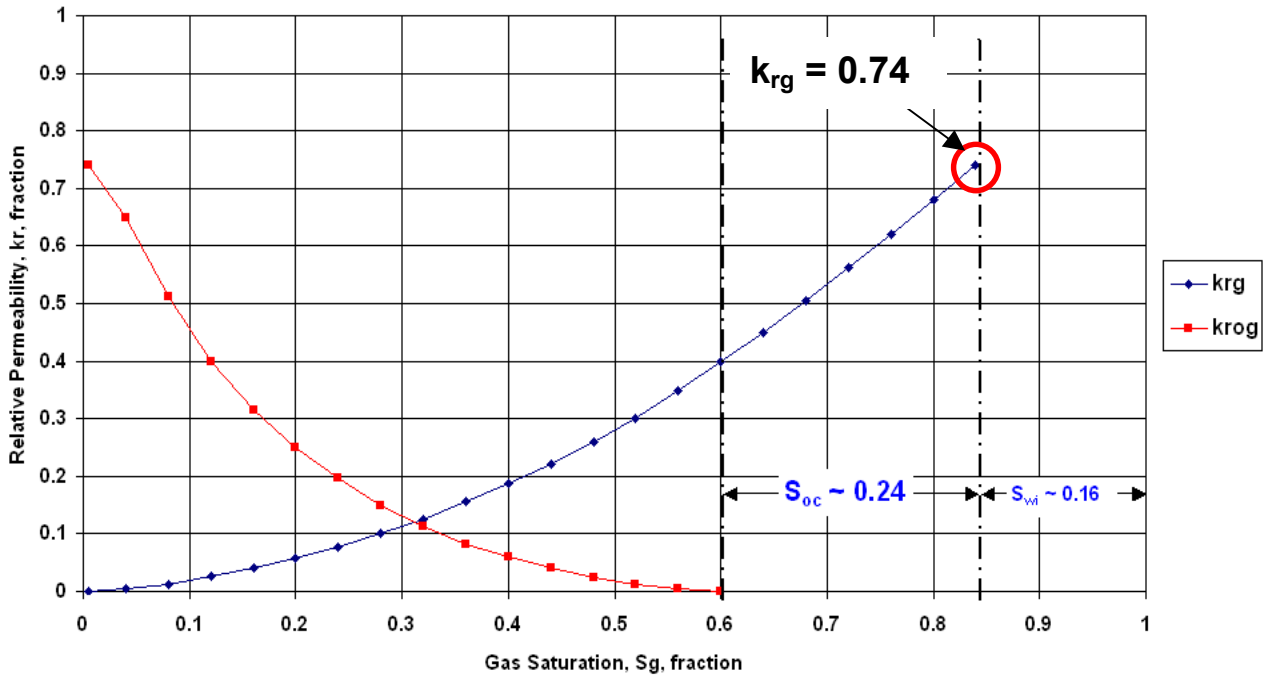

Fig. 4.3 – Gas-liquid relative permeability curves

Fig. 4.3 shows the relative permeability changes with gas saturation. At pressures above the dewpoint, the reservoir is primarily gas, and the gas relative permeability is at a maximum of 0.74. As the gas is produced, the pressure falls below the dewpoint and condensate starts to accumulate, thereby reducing the relative gas permeability. Once the critical oil saturation of 24% is attained, the oil relative permeability increases and the oil starts to move.

Upon completion of the reservoir description, a representative gas condensate reservoir fluid model was adopted. The details of the fluid model are given in the next section.

4.2 The fluid model

The reservoir fluid selected for this study was that from the third SPE Comparative Solution Project[23]. The fluid's pseudocomponents and composition are shown in **Table 4.2**. Due to its rich intermediates (C_2 – C_6 approx. 25%), the fluid model can be considered to be a rich gas condensate.

Table 4.2 – SPE3 condensate fluid model

Pseudocomponents	**Composition**
C_1	67.93
C_2	9.90
C_3	5.91
C_4	5.17
C_5	2.69
C_6	1.81
$C_7 – C_9$	3.99
$C_{10} – C_{11}$	1.22
$C_{12} – C_{14}$	0.80
$C_{15}+$	0.58
	100.00

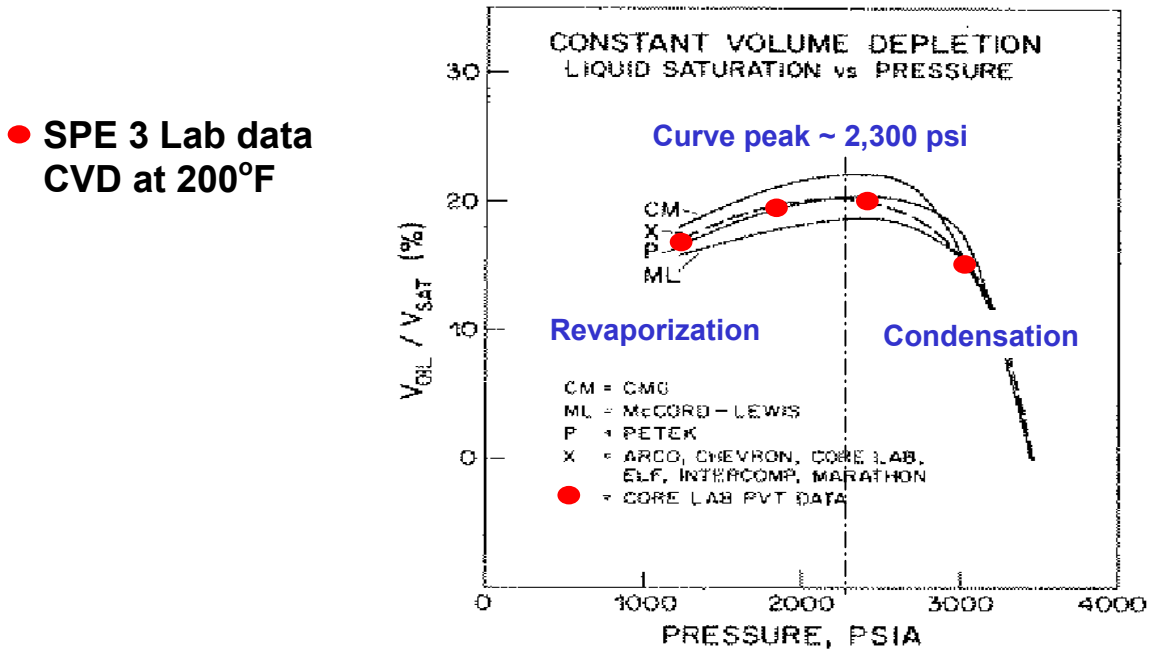

Fig. 4.4 – Constant-volume depletion test after SPE3[23]

In the same SPE comparative project, laboratory tests were done with the compositional fluid, including constant-composition expansion (CCE), constant-volume depletion (CVD) and swelling test. Of relevance to this work is the constant-volume depletion test, and **Fig. 4.4** shows that there is liquid dropout. With laboratory conditions at 200°F, at pressures below the dewpoint of 3,500 psi, there is condensation until about 2,300 psi, beyond which revaporization starts to occur. The revaporization starts at $S_o/(S_o+S_g)$ ratio of about 20%. With the water saturation included, the corresponding oil saturation is approximately 17%. This test gives an idea of what to expect in the simulation results, but does not predict what actually happens in the reservoir.

4.3 Simulation results

The simulations were done over a 15-year period, with the producer operating at different constant flowing bottomhole pressures (p_{wf}) of 3,500 psi; 3,000 psi; 2,500 psi; 2,000 psi; 1,500 psi; and 1,000 psi. Compositional simulation runs were made using CMG, and the results are presented in **Figs. 4.5 and 4.6**.

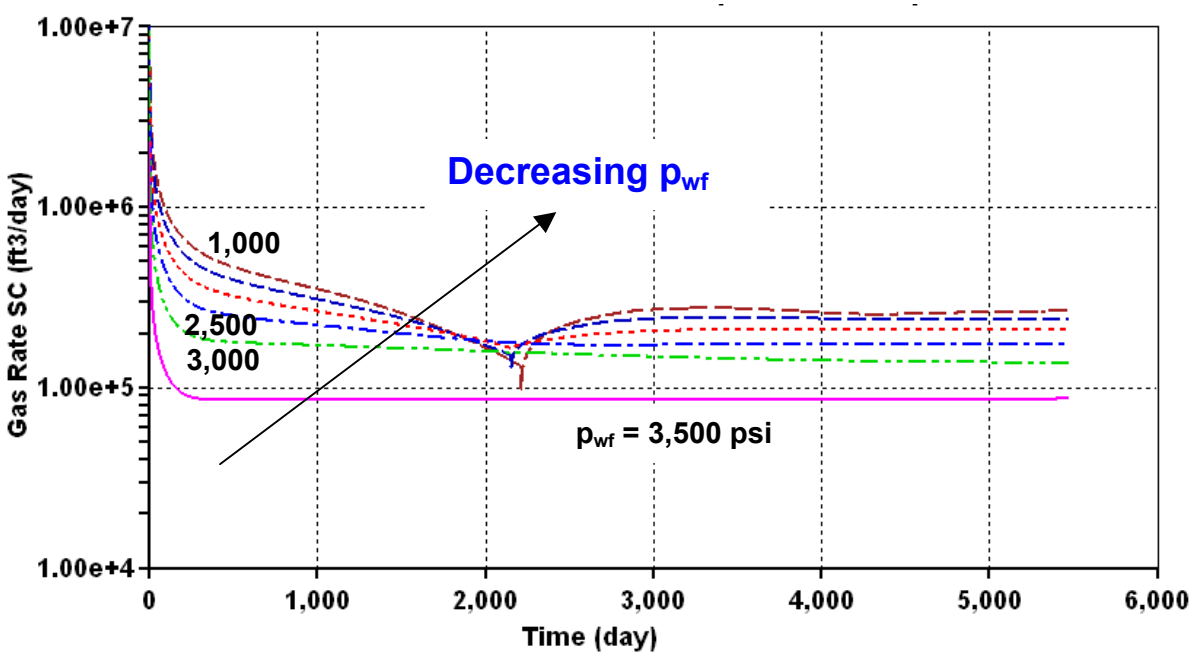

Fig. 4.5 – Gas rate reduction due to liquid build-up below dewpoint pressure of 3,500 psi

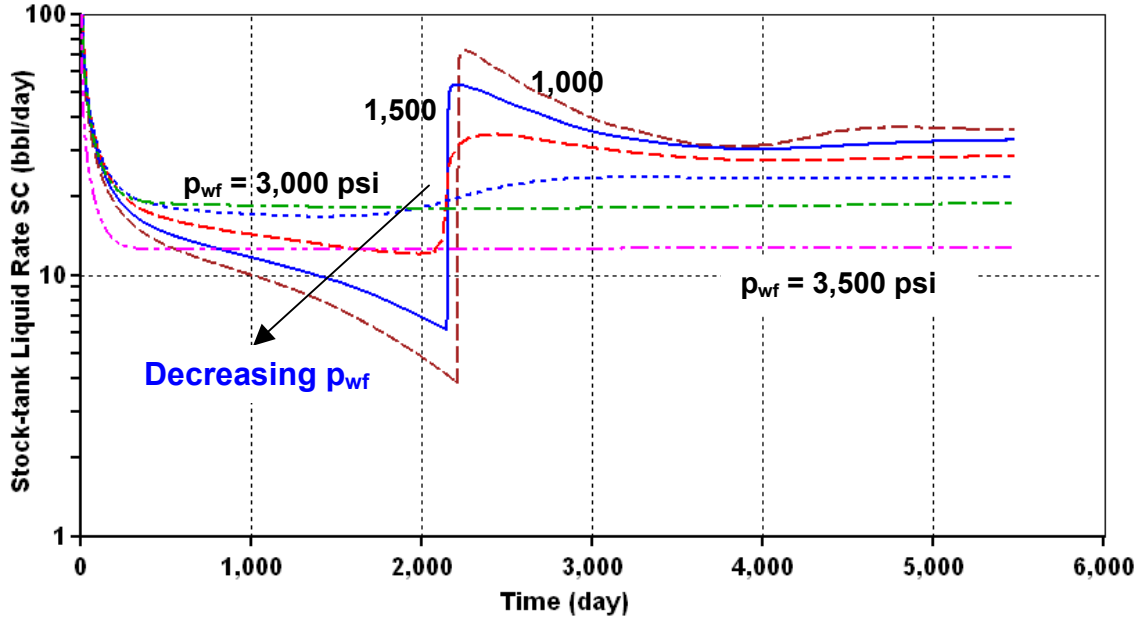

Fig. 4.6 – Liquid build-up due to reservoir below dewpoint pressure

Figs. 4.5 and 4.6 are for the same simulation runs. In Fig. 4.5, for a constant p_{wf} of 3,500 psi, there are transient effects until about 250 days, after which there is a steady gas production of about 85 Mscf/day. As the p_{wf} is reduced to 3,000 psi, the transient effects

are followed by a decrease in gas production. This decrease is due to liquid build-up, and the reduction in gas production becomes even more pronounced as p_{wf} decreases.

At about 2,159 days there is sharp change in gas production rate, which starts to increase. Fig. 4.6 also shows a sudden increase in stock-tank liquid rates for p_{wf} less than 3,000 psi. This anomaly can be ascribed to the effects of condensation and revaporization, plus the fact that the liquid that has accumulated near the wellbore is being produced.

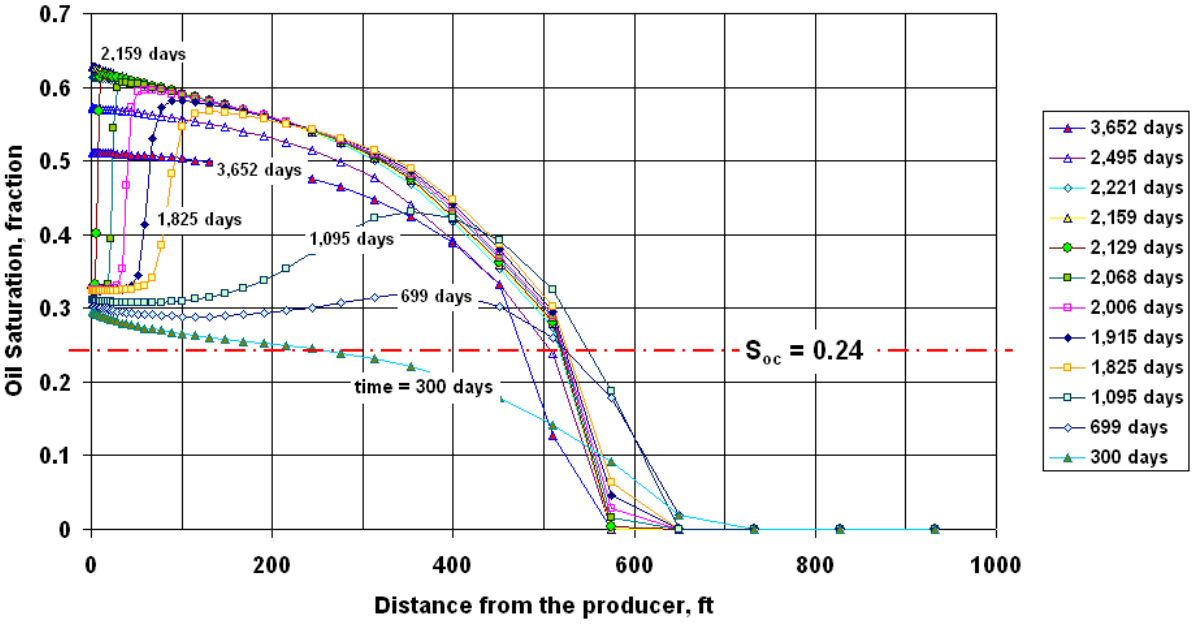

Fig. 4.7 – Oil saturation profile with p_{wf} at 1,500 psi

Fig. 4.7 shows the movement of the condensation front at a p_{wf} of 1,500 psi. The plot shows that revaporization starts to occur at about 699 days, and continues until the condensation front hits the wellbore at about 2,159 days. Beyond this time, the oil saturation close to the wellbore starts to drop, because the oil starts being produced with the gas. After the transient period (time greater than 300 days), it is noted that the oil saturation near the wellbore was always greater the critical oil saturation, and therefore the oil around the wellbore was always mobile.

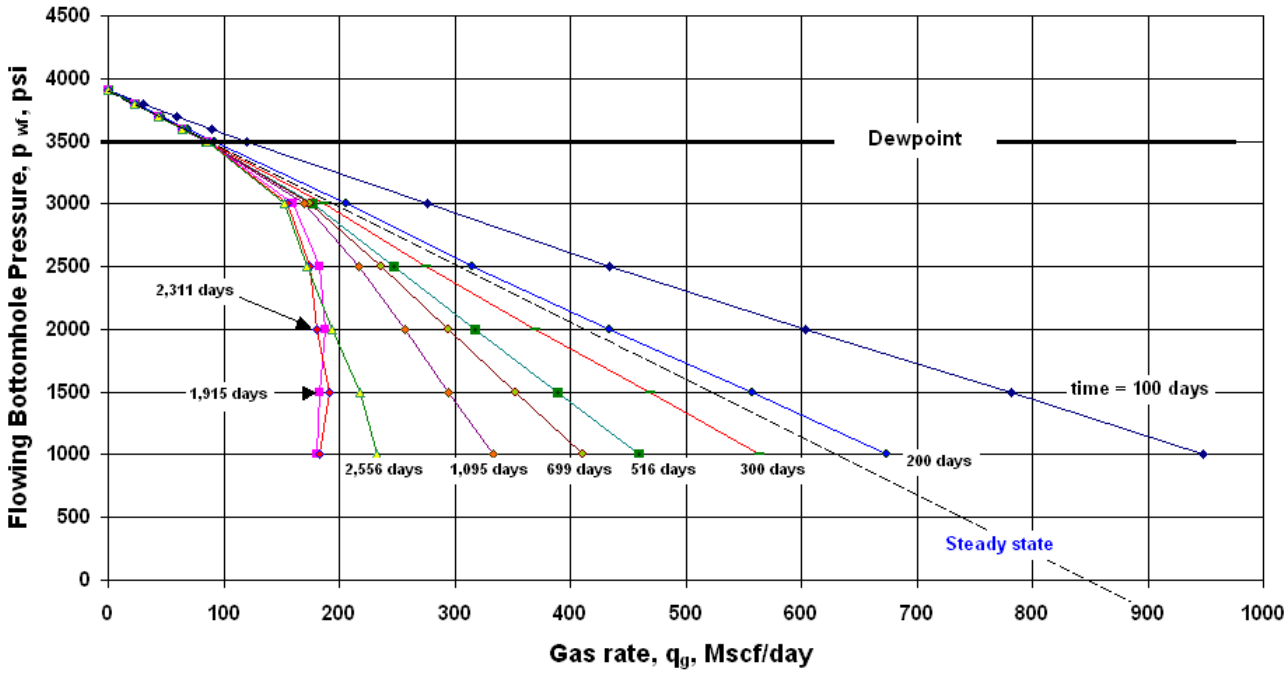

Fig. 4.8 – Gas inflow performance curves

In **Fig. 4.8**, the gas inflow performance curves helps to show the variation of flowing bottomhole pressure (p_{wf}) with gas rate (q_g). For p_{wf} above the dewpoint pressure, the relationship is a perfect straight line after transient because the reservoir only contains gas. The extrapolation of the straight line also helps to separate the transient from the steady state regime. For time earlier than 1,915 days, an increase in drawdown ($p_i - p_{wf}$), results in a corresponding increase in gas production. However between 1,915 and 2,311 days, there is a trend reversal, and more drawdown does not translate into any substantial increase in production. This raises the question of whether there is an optimum drawdown, which maximizes cumulative gas. The next section investigates the damage that results due to liquid build-up, and also answers the question that is raised.

4.4 Damage effects

At pressures below the dewpoint, the accumulation of liquid makes quantification of condensate damage a little more complicated. Dimensionless pseudopressure, m_D is introduced for simplicity, and used to develop the relation for dimensionless skin factor due to liquid build-up.

At steady state, Darcy's law can be expressed as:

$$q_g, scf/day = 0.00633\frac{k_g A}{B_g \mu_g}\frac{\left(p_i - p_{wf}\right)}{L} \quad \text{.....(4.1)}$$

$$q_g, scf/day = 0.00633\frac{k_g A}{2\mu_g}\left(\frac{2pT_{sc}}{zp_{sc}T}\right)\frac{\left(p_i - p_{wf}\right)}{L} \quad \text{.....(4.2)}$$

In terms of pseudopressure,

$$q_g, scf/day = 0.00633\frac{k_g A}{2}\frac{T_{sc}}{p_{sc}T}\frac{\left[m(p_i) - m(p_{wf})\right]}{L} \quad \text{.....(4.3)}$$

$$q_g, Mscf/day = \frac{0.00633}{1000}\frac{k_g A}{2T}\frac{520}{14.7}\frac{\left[m(p_i) - m(p_{wf})\right]}{L} \quad \text{.....(4.4)}$$

$$\frac{L}{A} = \frac{0.00633k_g A}{1000(2)}\frac{520}{14.7}\frac{\left[m(p_i) - m(p_{wf})\right]}{q_g} \quad \text{.....(4.5)}$$

To make the equation dimensionless, both sides are multiplied by $[2\pi h]$:

$$2\pi h\left(\frac{L}{A}\right) = 2\pi\frac{0.00633}{(2)1000}\frac{520}{14.7}k_g h\frac{\left[m(p_i) - m(p_{wf})\right]}{q_g T} \quad \text{.....(4.6)}$$

Combining the constant terms,

$$2\pi h\left(\frac{L}{A}\right) = \frac{1}{1422}k_g h\frac{\left[m(p_i) - m(p_{wf})\right]}{q_g T} \quad \text{.....(4.7)}$$

$$\text{So, } m_D = 2\pi h\left(\frac{L}{A}\right) \quad \text{.....(4.8)}$$

This implies that,

$$m_D = \frac{1}{1422} k_g h \frac{\left[m(p_i) - m(p_{wf})\right]}{q_g T} \quad \text{.....(4.9)}$$

For bottomhole flowing pressures above the dewpoint, there is no liquid build-up, and thus:

$$m_D = \frac{k_g h}{1422} \frac{\left[m(p_i) - m(p_{wf})\right]}{q_g T} \quad \text{.....(4.10)}$$

Eqn. 4.10 represents the dimensionless *m(p)*, for the undamaged case.

For pressures below the dewpoint, there is an accumulation of liquid due to condensate build-up, and therefore,

$$m_D = m_{D,undamaged} + s_c \quad \text{.....(4.11)}$$

Eqn. 4.11 represents the dimensionless *m(p)*, for the damaged case, and the term s_c is the dimensionless skin factor that quantifies damage that results due to condensate accumulation. For graphical illustration, **Figs. 4.9 – 4.11** show pseudopressure profiles for 300 days at p_{wf} = 3,500psi; 2,500 psi; and 1,500 psi respectively.

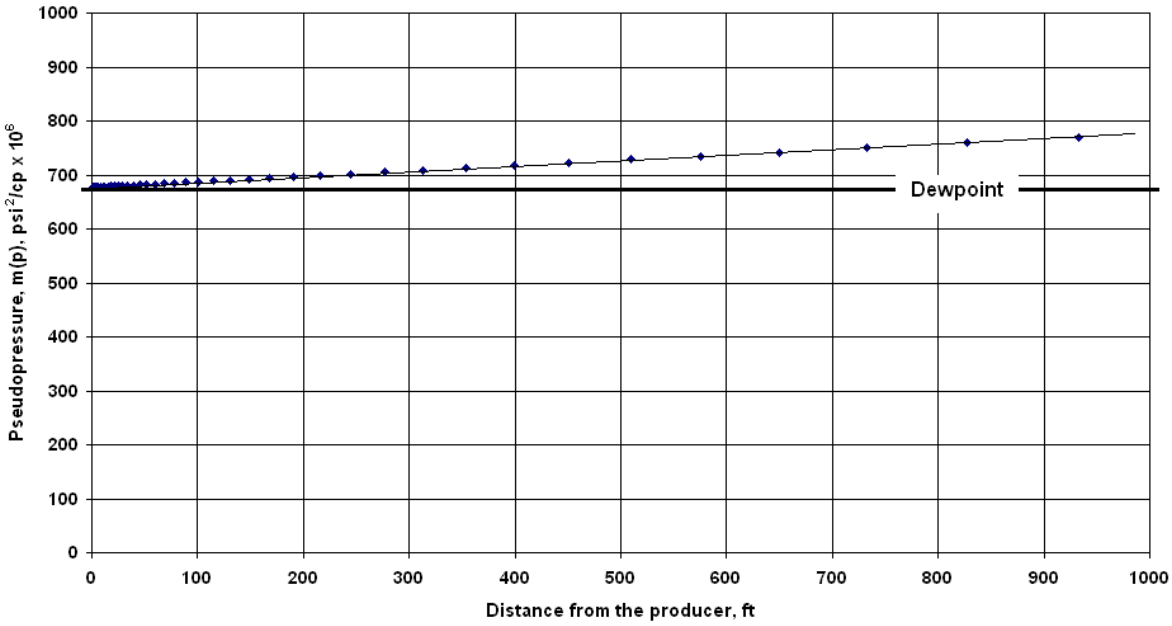

Fig. 4.9 – 300 days pseudopressure profile at p_{wf} = 3,500 psi

At pressures above and equal to the dewpoint pressure, the pseudopressure profile is a perfect straight line as shown in Figs. 4.9 – 4.11. The $\left[m(p_i) - m(p_{wf})\right]$ in the case of p_{wf} equal to 3,500 psi (Fig. 4.9) is approximately 92x10^6 psi^2/cp, while s_c is zero. At pressures below the dewpoint there is a deviation from the straight line due to skin, and the greater the drawdown, the greater s_c. The $\left[m(p_i) - m(p_{wf})\right]$ in the cases of p_{wf} equal to 2,500 psi (Fig. 4.10) and 1,500 psi (Fig. 4.11), are 332x10^6 psi^2/cp and 578x10^6 psi^2/cp respectively.

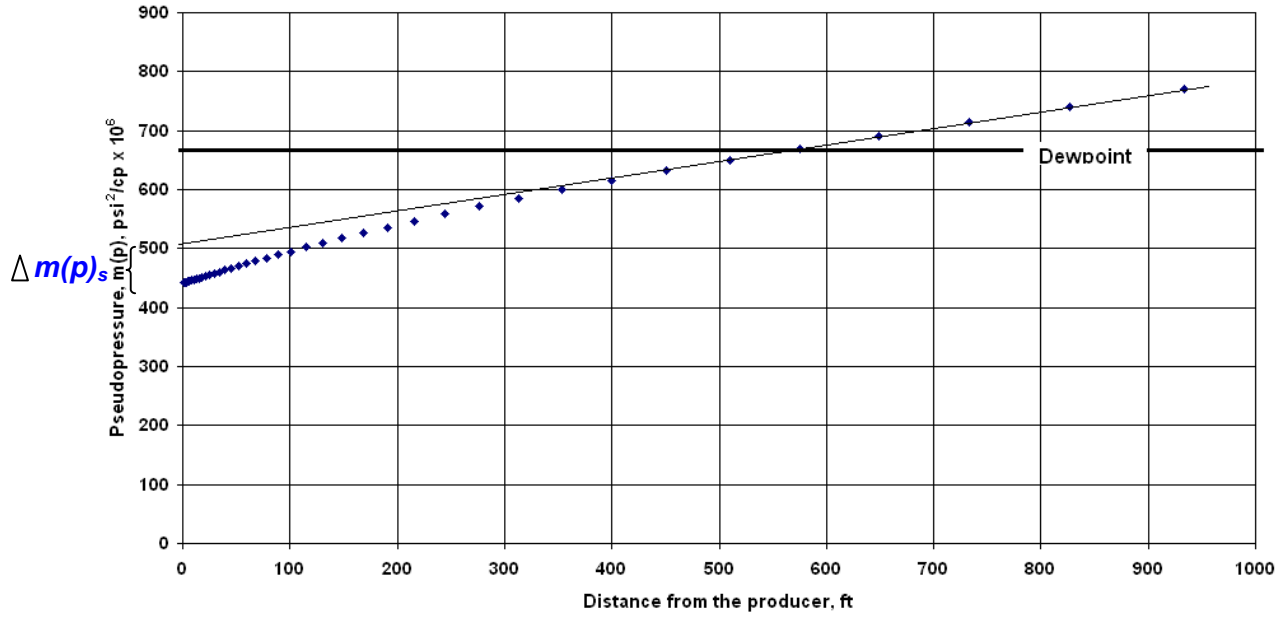

Fig. 4.10 – 300 days pseudopressure profile at p_{wf} = 2,500 psi

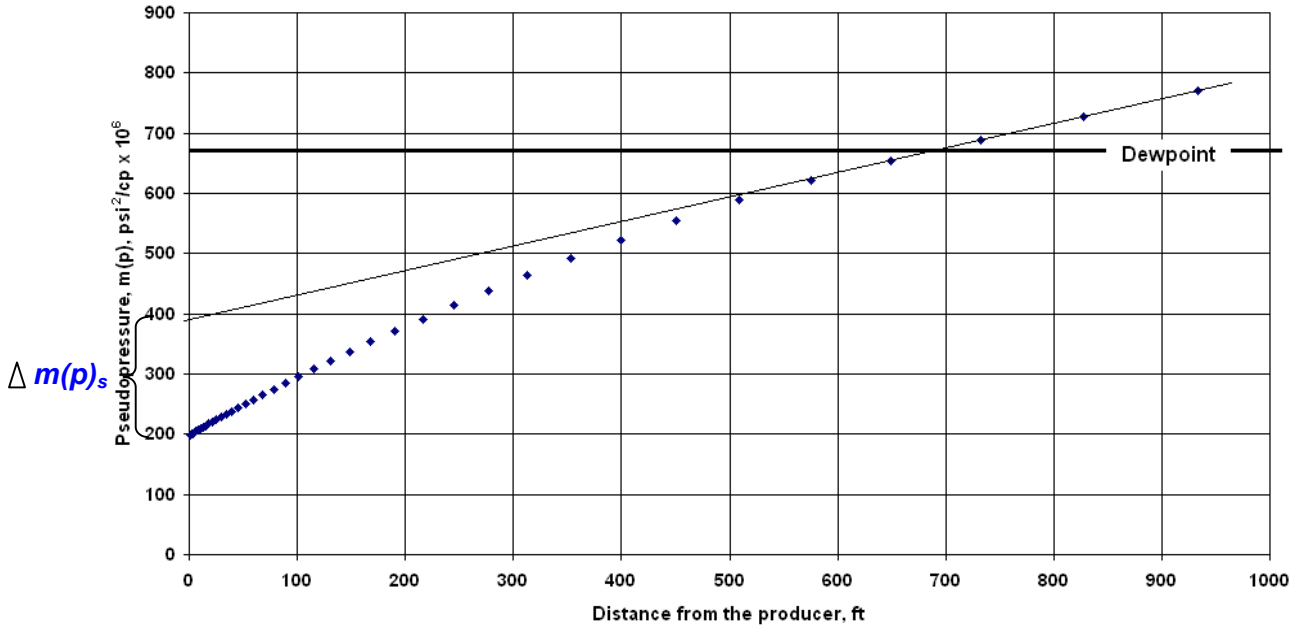

Fig. 4.11 – 300 days pseudopressure profile at p_{wf} = 1,500 psi

Table 4.3 provides a summary of similar results for $\left|m(p_i) - m(p_{wf})\right|$ for the different flowing bottomhole pressures. It also summarizes results for skin, on implementing Eqns. 4.10 and 4.11.

Table 4.3 – Pressure drop due to liquid build-up and associated skin factor at 300 days

p_{wf}, psi	$\Delta m(p)$, psi^2/cp x 10^6	$\Delta m(p)_s$, psi^2/cp x 10^6	Skin factor, s_c
3,500	92	0	0
3,000	210	25	0.38
2,500	332	65	0.85
2,000	457	120	1.02
1,500	578	190	0.99
1,000	680	240	0.85

In Table 4.3, the skin factor at pressures above the dewpoint was actually computed to be 0.02. In theory, the number is exactly zero, but whenever GasProp6 (software developed by Texas A&M Reservoir Simulation group) was used to compute pseudopressures, the z-factors computed could not be matched with that of CMG. To capture the variation of skin during the simulation, similar analysis was done at different times and the results are shown in **Fig. 4.12**.

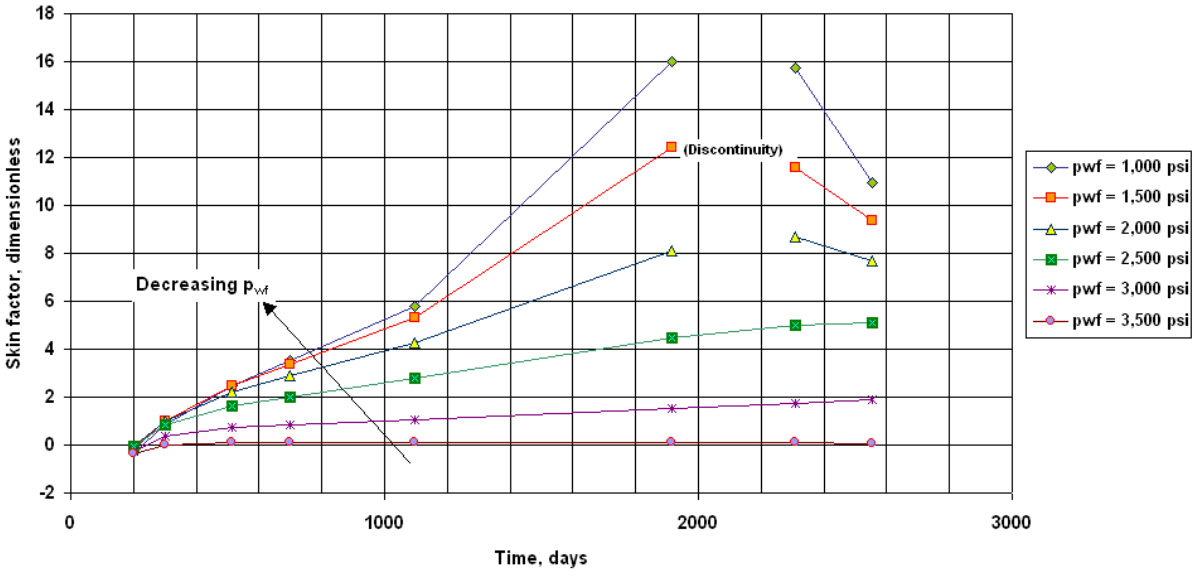

Fig. 4.12 – Skin factor variation with time at different p_{wf}

Fig. 4.12 shows that at p_{wf} equal to 3,500 psi, there is no damage due to liquid build-up. For drawdowns below the dewpoint pressure, there is an increase in condensate damage as time progresses. The most damage occurs when p_{wf} is 1,000 psi.

For the cases of p_{wf} at 1,000 psi and 1,500 psi, there is a trend reversal after 1,195 days, and the damage starts to decrease. The same trend reversal happens for p_{wf} at 2,500 psi, at about 2,311 days. The trends are due to the condensation and revaporization that happens near the fracture at the mentioned flowing bottomhole pressures. To investigate the effect the skin as on overall production, a cumulative production plot is made as shown in **Fig. 4.13**.

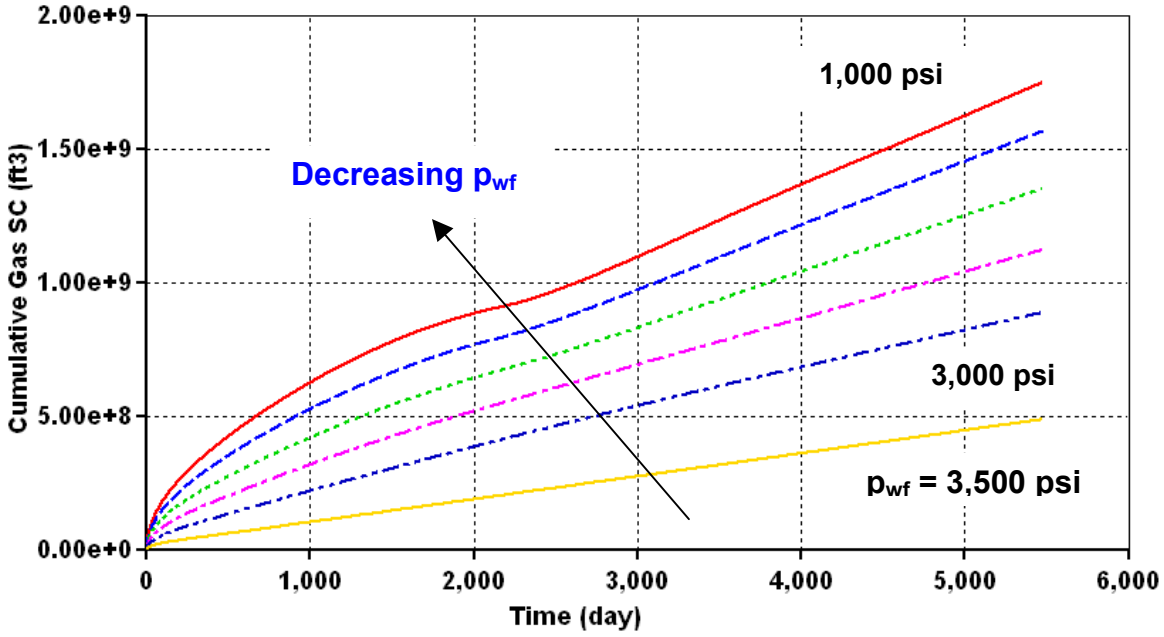

Fig. 4.13 – Cumulative gas production

From Fig. 4.13, the most cumulative production occurs for p_{wf} of 1,000 psi, and the least is when p_{wf} is at 3,500 psi. Even though, the condensate damage is most severe at p_{wf} of 1,000 psi, the damage does not stop the cumulative gas production from being the largest. To answer the question raised earlier in the chapter, the optimum drawdown resulting in most production is when p_{wf} is the lowest. The summary and recommendations are made in the next chapter.

CHAPTER V
SUMMARY AND DISCUSSION

This chapter discusses the results obtained in this work and provides recommendations for improvement on similar projects in the future. The most relevant results were obtained in Chapter IV, and thus, the summary in this chapter will simply be further expatiations on discussions in the previous chapter.

5.1 Summary

Compositional simulations were done over a 15-year period using a linear model to represent the hydraulic fracture and fluid adopted from SPE3[23]. With the producer operating at different constant flowing bottomhole pressures (p_{wf}) of 3,500 psi; 3,000 psi; 2,500 psi; 2,000 psi; 1,500 psi; and 1,000 psi, and an injector at 3,910 psi, the results were presented in Figs. 4.5 - 4.13, and each illustration was adequately discussed. The overall summary was that the most cumulative production occurs for p_{wf} of 1,000 psi, and the least is when p_{wf} is at 3,500 psi. The condensate damage does not prevent the lowest drawdown, p_{wf} = 1,000 psi, from producing the highest cumulative gas.

An important note is that the 1-D model used for condensate simulation is analogous to a hydraulic fracture propagating to the entire extent of the reservoir, and assumes linear flow into an infinite conductivity fracture. In the case where the fracture does not propagate to the entire reservoir extent, the productivity is not the same. It is expected that as the fracture half-length is halved, the productivity will be doubled. However more work needs to be done to validate this expectation.

It is also noted that the gas-liquid relative permeabilities are assumed to be constant throughout the simulations runs. The assumption is a general practice in reservoir engineering, but in the field this is not likely to happen. This is because, gas relative permeability is a function of gas saturation, and the gas saturation in the reservoir keeps changing with time.

5.2 Recommendations for future work

In field operations, optimum drawdown depends on the economics of the project and the environmental conditions surrounding the project. Work done in this project uses idealized field data, and therefore it will be helpful to do the same work with actual field data, to see if similar conclusions can be reached.

In the idealized case studied, an injector well was used to eliminate the effects of depletion, but in the field, this will not be realistic. Future work on this project without an injector, could lead to some interesting results that might be of greater relevance in field operations where depletion exists.

The 1-D model used for condensate simulation is analogous to a hydraulic fracture propagating to the entire extent of the reservoir, and assumes linear flow into an infinite conductivity fracture. Future work should consider cases where the fracture does not propagate to the entire reservoir extent, and pseudoradial flow is observed.

Lastly, the project could be done using different condensate fluid models besides that adopted from the third SPE comparative solution project. This will help to generalize the conclusions that have been reached, regardless of whether the fluid is a rich gas condensate or a lean gas condensate. Perhaps some general correlations could be developed.

CHAPTER VI
CONCLUSIONS

This chapter is a summary of the conclusions reached in this work. The project set out to improve the management of hydraulic fractured wells in gas condensate reservoirs by understanding the mechanics of liquid build-up and to specify appropriate drawdown. It also set out to provide methodology for quantifying the condensate damage that impairs linear flow of gas into the hydraulic fracture using dimensionless skin factor.

The following main conclusions can be drawn from this work:

1. The optimum drawdown corresponds to the lowest p_{wf} giving the largest cumulative gas production. The condensate damage does not prevent the lowest drawdown, p_{wf} = 1,000 psi, from producing the highest cumulative gas.
2. The more the large drawdown, the larger the cumulative production. However, there is a period of trend reversal within which more drawdown does not necessarily translate into higher gas production rate for the cases studied. This period is short and has small effect on cumulative production.
3. The sudden increase in stock-tank liquid rates for p_{wf} less than 3,000 psi is due to the effects of condensation and revaporization, plus the fact that the liquid that has accumulated reaches the fracture and is produced. The liquid front moves towards the producer from the injector, and once it reaches the wellbore, the oil starts being produced as liquid at the perforations. Earlier stock-tank liquid production was from the condensation of the reservoir gas.
4. For flowing bottomhole pressure below the dewpoint pressure, there is a decrease in gas production due to liquid build-up, until about 2,000 days. Like in the increase in stock-tank liquid scenario, the gas production also increases due to the effects of condensation and revaporization.

Considering the recommendations that have been mentioned in the Chapter V could help further improve the conclusions. In all, the project has been a very interesting one. It is different from similar work considering radial flow into the wellbore, and serves as a

base foundation for future work with respect to gas condensate damage in hydraulically fractured wells.

NOMENCLATURE

A Drainage area, ft^2

A_c Area of fracture face subject to damage, ft^2

B Formation volume factor, rb/stb

C_D Dimensionless wellbore storage, dimensionless

c_t Compressibility, psi^{-1}

h Reservoir thickness, ft

k Reservoir permeability, md

k_g Effective gas permeability, md

k_{rog} Oil relative permeability, fraction

k_{rg} Gas relative permeability, fraction

k_s Damaged zone permeability, md

kh Conductivity, md-ft

L Reservoir length, ft

m_D Dimensionless pseudopressure, dimensionless

m_{DS} Dimensionless pseudopressure with skin, dimensionless

$m(p)$ Real gas pseudopressure, psi^2/cp

p_i Initial reservoir pressure, psi

p_d Dewpoint pressure, psi

p_{wf} Flowing bottomhole pressure, psi

p_{inj} Injection pressure, psi

p_D Dimensionless pressure, dimensionless

q_g Gas production rate, stb/day

r_w Wellbore radius, ft

r_s Damaged zone radius, ft

s Skin factor, dimensionless

s_{ff} Fracture face skin, dimensionless

S_{cc} Critical condensate saturation, fraction

S_{oc} Critical oil saturation, fraction

T Temperature, ^oF

t Time, days

t_D Dimensionless time, dimensionless

w_s Width (extent) of damage on the fracture, ft

x_f Fracture half-length, ft

x_e Reservoir extent, ft

ϕ Porosity, fraction

μ Viscosity, cp

REFERENCES

1. Li, K. and Firoozabadi, A.: "Phenomenological Modeling of Critical Condensate Saturation and Relative Permeabilities in Gas/Condensate Systems," *SPEJ* (June 2000) **20** 138.

2. Saad, N., Cullick, A.S., and Honarpour, M.M.: "Effective Relative Permeability in Scale-Up and Simulation," paper SPE 29592 presented at the 1995 SPE Rocky Mountain Regional/Low-Permeability Reservoirs Symposium, Denver, 20-22 March.

3. Bardon, C., Longeron, D.G., Baudoin, F., Delhomme, A., and Naili N.: "Gas/Oil Relative Permeabilities and Residual Oil Saturations in a Field Case of a Very Light Oil, in the Near-Miscibility Conditions," paper SPE 28625 presented at the 1994 Annual Technical Conference and Exhibition, New Orleans, 25-28 September.

4. Henderson, G.D., Danesh, A., Tehrani, D.H., and Peden, J.M.: "The Effect of Velocity and Interfacial Tension on Relative Permeability of Gas Condensate Fluids in the Wellbore Region," *SPEJ* (1997) 265.

5. Haniff, M.S. and Ali, J.K.: "Relative Permeability and Low Tension Fluid Flow in Gas Condensate Systems," paper SPE 20917 presented at the 1990 Europec 90, The Hague, The Netherland, 22-24 October.

6. Blom, S.M.P., Hagoort, J., and Soetekouw, D.P.N.: "Relative Permeability at Near-Critical Conditions," paper SPE 38935 presented at the 1997 SPE Annual Technical Conference and Exhibition, San Antonio, Texas, 5-8 October.

7. Barnum, R.S., Brinkman, F.P., Richardson, T.W., and Spillette, A.G.: "Gas Condensate Reservoir Behavior: Productivity and Recovery Reduction due to Condensation," paper SPE 30767 presented at the 1995 SPE Annual Technical Conference and Exhibition, Dallas, 22 – 25 October.

8. El-Banbi, A.H., McCain, W.D. and Semmelbeck, M.E.: "Investigation of Well Productivity in Gas-Condensate Reservoirs," paper SPE 59773 presented at the 2000 SPE/CERI Gas Technology Symposium, Calgary, 3 – 5 April.

9. Kroemer, E., Abou-Sayed, I.S., Babu, D.K. and Cohen, M.F.: "Compositional Simulation of Well Performance for Fractured and Multiple Fractured Horizontal Wells in Stratified Gas Condensate Reservoirs," paper SPE 37995 presented at the 1997 SPE Reservoir Simulation Symposium, Dallas, 8 – 11 June.

10. Valko, P. and Economides, M.J.: "Hydraulic Fractures Mechanics," John Wiley & Sons, 1995.

11. Al-Hashim, H.S., and Hashmi, S.S.: "Long-Term Performance of Hydraulically Fractured Layered Rich Gas Condensate Reservoir," paper SPE 64774 presented at the 2000 SPE International Oil and Gas Conference and Exhibition, Beijing, 7 – 10 November.

12. Romero, D.J., Valko, P. and Economides, M.J.: "The Optimization of the Productivity Index and the Fracture Geometry of a Stimulated Well with Fracture Face and Choke Skins," paper SPE 73758 presented at the 2002 SPE International Symposium and Exhibition on Formation Damage Control, Lafayette, Louisiana, 20 – 21 February.

13. Wang, X., Indriati, S., Valko, P. and Economides, M.J.: "Production Impairment and Purpose-Built Design of Hydraulic Fractures in Gas-Condensate Reservoirs," paper SPE 64749 presented at the 2000 SPE International Oil and Gas Conference and Exhibition, Beijing, 7 – 10 November.

14. Rahman, M.M., Rahman, M.K., and Rahman, S.S.: "Control of Hydraulic-Fracturing-Induced Formation Damage by Optimizing Treatments with Constraints," paper SPE 73754 presented at the 2002 SPE International Symposium and exhibition on Formation Damage Control, Lafayette, Louisiana, 20 – 21 February.

15. Indriati, S., Wang, X., and Economides, M.J.: "Adjustment of Hydraulic Fracture Design in Gas-Condensate Wells," paper SPE 73751 presented at the 2002 SPE International Symposium and exhibition on Formation Damage Control, Lafayette, Louisiana, 20 – 21 February.

16. Poe, B.D.: "Production Performance Evaluation of Hydraulically Fractured Wells," paper SPE 59758 presented at the 2000 SPE/CERI Gas Technology Symposium, Calgary, 3 – 5 April.

17. Metcalfe, R.S., Vogel, J.L., and Morris, R.W.: "Compositional Gradients in the Anschutz Ranch East Field," paper SPE 14412 presented at the 1988 Reservoir Engineering Conference, August.

18. Creek, J.L. and Schrader, M.L.: "East Painter Reservoir: An Example of a Compositional Gradient From a Gravitational Field," paper SPE 14411 presented at the 1985 SPE Annual Technical Conference and Exhibition, Las Vegas, Nevada, 22-25 September.

19. Fevang, O., Kameshwar, S., and Whitson, C.H.: "Guidelines for choosing Compositional and Black-oil Models for Volatile Oil and Gas Condensate Reservoirs," paper SPE 63087 presented at the 2000 SPE Annual Technical Conference and Exhibition, Dallas, Texas, 1-4 October.

20. Bennion, D.B., Thomas, F.B., Imer, D. and Ma, T.: Low Permeability Gas Reservoirs and Formation Damage – Tricks and Traps," paper SPE 50753 presented at the 2000 SPE SPE/CERI Gas Technology Symposium, Calgary, 3 – 5 April.

21. Whitson, C.H., Fevang, O., and Saevareid, A.: "Gas Condensate Relative Permeability for Well Calculations," paper SPE 56476 presented at the 1999 SPE Annual Technical Conference and Exhibition, Houston, 3-6 October.

22. Lee, J. and Wattenbarger, R.A.: "Gas Reservoir Engineering," Society of Petroleum Engineers Inc., 1996.

23. Kenyon, D.E. and Behie, G.A.: "Third SPE Comparative Solution Project: Gas Cycling of Retrograde Condensate Reservoirs," *JPT* (August 1987) 981.

24. Zapata, J.F.: "Impact of Relative Permeability Models on Fluid Flow Behavior for Gas Condensate Reservoirs," Master of Science thesis, Petroleum Engineering Department, Texas A&M U., August 2002.

APPENDIX A

GASSIM DATA FILE FOR HAWKINS' APPROACH

```
CMNT
CMNT  Homogeneous  Cylindrical  Reservoir
CMNT  Radial  Flow,  Constant-rate  production,  Infinite-acting
CMNT  Slightly  Compressible  Fluid
CMNT
CMNT  Geometrically  spaced  grid  system
CMNT
CMNT  Single  Value  Input  Data
IMAX  20
JMAX  1
RWEL  0.5
CROC  0.000015
PREF  3000
NEWT  1
BETA  0
CMNT  Bo,  rcf/scf  mo,  cp
CNST  1.475  0.72
END
CMNT  Grid  Input  Data
CMNT  b  =  1.54
RR    -1
  0.772462787300798  1.19339751552904  1.84371034240682
2.84839526014176  4.40055868396697  6.79853565339572  10.5032316007718
16.2267111159961  25.0690609947743  38.7298334620742
  59.8347102156191  92.4401740609854  142.81318902744  220.635748118903
340.86580994025  526.61230728398  813.576821422975  1256.91563831943
1941.84111475638  3000
DELY  150
KX    0.1
KY    0.1
PHI   0.23
POI   3000
WIND  1  3  1  1
KX    0.02
END
CMNT  Schedule  Data
CMNT  Well  No.  i  -  location  j  -  location  skin
NAME  1  1  1  0
CMNT  Well  No.  scf/D
QG    1  112.2917
ALPH  1.2
DELT  0.01
DTMX  50
WELL  1
PMAP  2
TIME  200
END
```

APPENDIX B

GASSIM DATA FILE FOR FRACTURE FACE SKIN SIMULATION

```
CMNT
CMNT  An  infinite  conductivity  vertical  fracture
CMNT
CMNT  Single  Value  Data
CMNT
IMAX  21
JMAX  16
CROC  0.0000071111
GRAV  0.58
PREF  4859
TSC   520
PSC   14.7
T     743
NEWT  1
BETA  0
TABL  0
IMAP  0
CNST  1  1
END
CMNT
CMNT  Grid  Data
CMNT
CMNT  Global  Data
H     200
KX    2
KY    2
PHI   0.15
POI   4859
DELX  -1
  0.01  46.669  46.669  46.669  46.669  46.669  46.669  46.669  46.669
46.669  46.669  46.669  46.669  46.669  46.669  46.669  46.669  46.669
46.669  46.669  46.669
DELY  -1
  0.01  0.5  0.798183703219349  1.27419444816991  2.03408248652358
3.24714298349402  5.18363322289597  8.2749831239639  13.2099133479262
21.0878751105089  33.6639964974663  53.7401067790217  85.7889548805655
136.950691403775  218.62362004623  349.00362131944
CMNT
CMNT  Infinite  Conductivity  Fracture
WIND  2  11  1  1
PHI   0.3
KX    1450000
KY    1450000
CMNT  Modelling  the  fracture  face  skin  at  j = 2
CMNT  2  11  2  2
CMNT  0.15
CMNT  0.01
CMNT  0.01
CMNT  Well  cell  with  wellbore  storage  Vwb'286.722  rcf.
CMNT  Porosity  is  chosen  accordingly.
WIND  1  1  1  1
PHIS  924.55
```

```
KX    725000
KY    725000
END
CMNT
CMNT  Schedule  Data
CMNT
WELL  1
PMAP  1
PLOT  2
DIMP  0
NAME  1  1  1  0
ALPH  1.5
DTMX  20
DTMN  0.00001
QG    1  2000
TIME  10
TIME  100
TIME  365
END
```

APPENDIX C

DEVELOPING AN ANALYTICAL SOLUTION FOR FRACTURE FACE SKIN

The 1-D linear model is analogous to linear flow in an infinite conductivity the hydraulic fracture. **Fig. C.1** gives an illustration.

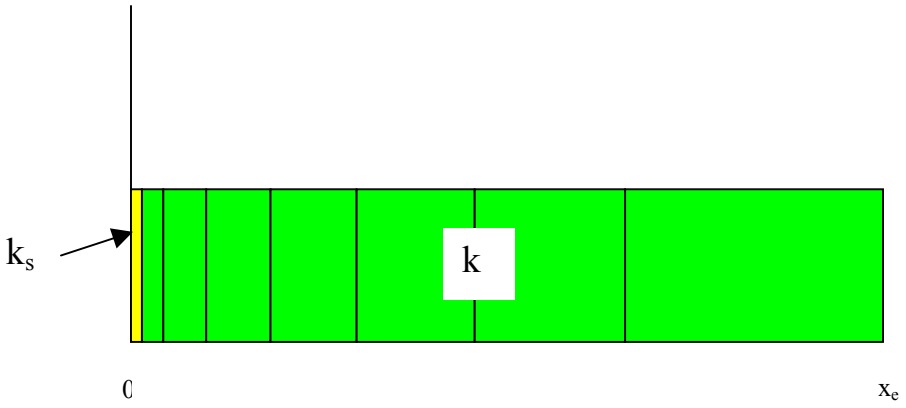

Fig. C.1 – Schematic of a linear model

Recall Darcy's law,

$$q = \frac{CkA_c \Delta p}{B\mu x_e} \qquad \text{.....(C.1)}$$

where C is a conversion constant,

Eqn. (C.1) implies that,

$$\Delta p = \frac{qB\mu x_e}{kA_c} \qquad \text{.....(C.2)}$$

For the no damage case:

$$p_e - p_o = \frac{qB\mu x_e}{kA_c} \qquad \text{.....(C.3)}$$

For a damaged case:

$$p_e - p_{os} = \left(p_e - p_s\right) + \left(p_s - p_{os}\right) \quad \text{.....(C.4)}$$

$$p_e - p_o = \frac{qB\mu\left(x_e - x_s\right)}{kA_c} + \frac{qB\mu\left(x_s - 0\right)}{kA_c} \quad \text{.....(C.5)}$$

$$p_e - p_{os} = \frac{qB\mu}{A_c}\left(\frac{x_e - x_s}{k} + \frac{x_s}{k_s}\right) \quad \text{.....(C.6)}$$

NOTE: Pressure drop due to skin, $\Delta p_s = p_o - p_{os}$

$$p_o - p_{os} = p_o - p_e + p_e - p_{os} \quad \text{.....(C.7)}$$

Rearranging,

$$p_o - p_{os} = \left(p_e - p_{os}\right) - \left(p_e - p_o\right) \quad \text{.....(C.8)}$$

Substituting Eqns. (C.3) and (C.6)

$$p_o - p_{os} = \frac{qB\mu}{A_c}\left(\frac{x_e - x_s}{k} + \frac{x_s}{k_s} + \frac{x_e}{k}\right) \quad \text{.....(C.9)}$$

$$p_o - p_{os} = \frac{qB\mu}{A_c}\left(\frac{x_s}{k_s} - \frac{x_s}{k}\right) \quad \text{.....(C.10)}$$

$$p_o - p_{os} = \frac{qB\mu}{A_c} x_s \left(\frac{1}{k_s} - \frac{1}{k}\right) \quad \text{.....(C.11)}$$

$$\Delta p_s = \frac{qB\mu}{A_c} x_s \left(\frac{1}{k_s} - \frac{1}{k}\right) \quad \text{.....(C.12)}$$

$$\Delta p_s = \frac{qB\mu}{A_c} x_s \left(\frac{k - k_s}{k k_s} \right) \quad \text{..... (C.13)}$$

For linear flow, at steady-state, the infinite-acting analytical solution can be written as:

$$p_{WD} = \frac{1}{2} \ln t_D + 0.4045 + s \quad \text{..... (C.14)}$$

In terms of field parameters,

$$\text{Dimensionless pressure, } p_{WD} = \frac{kh\left(p_i - p_{wf}\right)}{141.2 q_o B_o \mu_o} \quad \text{..... (C.15)}$$

$$\text{Dimensionless time, } t_{DXe} = \frac{0.00633kt}{\phi \mu_o c t x_e^{\,2}} \quad \text{..... (C.16)}$$

$$\text{Skin factor, } s = p_{WD,skin} = \frac{kh\left(\Delta p_s\right)}{141.2 q_o B_o \mu_o} \quad \text{..... (C.17)}$$

Substituting for Δp_s from Eqn. (C.13),

$$\text{Skin factor, } s = p_{WD,skin} = \frac{kh}{141.2 q_o B_o \mu_o} \frac{qB\mu}{A_c} x_s \left(\frac{k - k_s}{k k_s} \right) \quad \text{..... (C.18)}$$

For a single-phase oil system,

$$s = \frac{kh}{141.2} \frac{1}{A_c} x_s \left(\frac{k - k_s}{k k_s} \right) \quad \text{..... (C.19)}$$

In relation to hydraulic fractures, A_c represents the area of fracture face subject to damage, and x_s represents the width (extent) of damage on the fracture, w_s.

Fracture face damage implies permeability reduction normal to the fracture face and it includes permeability impairments caused by the filter cake, polymer-invaded zone, and filter cake-invaded zone. The fracture face skin effect is illustrated in **Fig. C.2**.

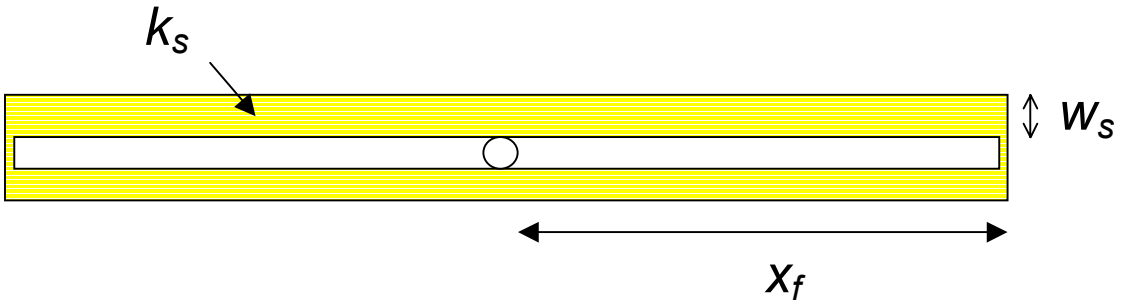

Fig. C.2 – Fracture face damage

Substituting with parameters in Fig. C.2,

$$\text{Fracture face skin, } s_{ff} = \frac{kh}{141.2}\frac{1}{4x_f h}w_s\left(\frac{k-k_s}{kk_s}\right) = \frac{1}{141.2}\left[\frac{ws}{4xf}\left(\frac{k}{k_s}-1\right)\right] \quad \text{.....(C.20)}$$

$$s_{ff} = \frac{1}{141.2}\left[\frac{ws}{4xf}\left(\frac{k}{k_s}-1\right)\right] \quad \text{.....(C.21)}$$

In terms of Darcy Units,

$$s_{ff} = \frac{1}{141.2}x\frac{1}{0.00633}x\frac{5.615scf}{1bbl}\left[\frac{ws}{4xf}\left(\frac{k}{k_s}-1\right)\right] \quad \text{.....(C.22)}$$

$$s_{ff} = 2\pi\left[\frac{ws}{4xf}\left(\frac{k}{k_s}-1\right)\right] \quad \text{.....(C.23)}$$

$$s_{ff} = \frac{\pi w_s}{2xf}\left(\frac{k}{ks} - 1\right) \quad \text{..... (C.24)}$$

Eqn. (C.24) is the fracture face skin formula.

APPENDIX D

CMG SPE3 COMPARATIVE SOLUTION PROJECT (GMFLU001.DAT)

```
RESULTS SIMULATOR GEM
RESULTS SECTION INOUT
*TITLE1  'SPE3'
*TITLE2  'Cycling in Gas Condensate Reservoir'
*TITLE3  'Modified Relative Permeabilities'
*CASEID  'CASE 1'
*INUNIT *FIELD

*WRST 0
*WPRN *ITER  *BRIEF
*WSRF *WELL 1
*WSRF *GRID 10
*OUTPRN *GRID PRES SO SG SW

*OUTSRF *WELL     *PAVG
                  *SO 7 3 1
                  *Y 'C1' 1 9 4
                  *RMOL 'C1' 1 9 4
                  *ZWEL 'C1' 'PROD'

*OUTSRF *GRID PRES SO SG SW RHOO RHOG SIG VISO




GRID CART 9 9 4
KDIR UP
DI CON 293.3

DJ CON 293.3

DK KVAR
       2*50. 2*30.


DEPTH TOP 1 1 1 7425.



**$ RESULTS PROP NULL  Units: Dimensionless
**$ RESULTS PROP Minimum Value: 1  Maximum Value: 1
**$ 0 = NULL block, 1 = Active block
NULL CON 1.

**$ RESULTS PROP PINCHOUTARRAY  Units: Dimensionless
**$ RESULTS PROP Minimum Value: 1  Maximum Value: 1
**$ 0 = PINCHED block, 1 = Active block
PINCHOUTARRAY CON 1.
RESULTS SECTION GRID
RESULTS SECTION NETPAY
```

```
RESULTS SECTION NETGROSS
RESULTS SECTION POR

**$ RESULTS PROP POR  Units: Dimensionless
**$ RESULTS PROP Minimum Value: 0.13  Maximum Value: 0.13
POR CON 0.13
RESULTS SECTION PERMS

**$ RESULTS PROP PERMI  Units: md
**$ RESULTS PROP Minimum Value: 20  Maximum Value: 150
PERMI IJK
      1:9 1:9 1:1 150
      1:9 1:9 2:2 20
      1:9 1:9 3:3 40
      1:9 1:9 4:4 130

**$ RESULTS PROP PERMJ  Units: md
**$ RESULTS PROP Minimum Value: 20  Maximum Value: 150
PERMJ EQUALSI

**$ RESULTS PROP PERMK  Units: md
**$ RESULTS PROP Minimum Value: 2  Maximum Value: 15
PERMK EQUALSI * 0.1
RESULTS SECTION TRANS
RESULTS SECTION FRACS
RESULTS SECTION GRIDNONARRAYS
CPOR  MATRIX   4.E-06
PRPOR MATRIX   3550.

RESULTS SECTION VOLMOD
RESULTS SECTION SECTORLEASE

RESULTS SECTION ROCKCOMPACTION
RESULTS SECTION GRIDOTHER
RESULTS SECTION MODEL
*MODEL        *PR
*NC           10  10
*COMPNAME     'C1'        'C2'        'C3'        'C4'        'C5'
              'C6'        'C7-9'      'C10-11'    'C12-14'    'C15+'
*HCFLAG       0           0           0           0           0
              0           0           0           0           0
*TRES         200.
*PCRIT         40.000000   48.200000   42.010000   37.470000
33.310000
               29.920000   26.253000   23.184000   19.987000
12.554400
*TCRIT         194.44600   305.43000   369.90000   425.20000
469.60000
               507.90000   573.45000   637.79000   685.75000
748.33100
*AC             0.013000    0.098600    0.152400    0.201000
0.253900
                0.300700    0.361300    0.450100    0.533900
0.724400
*VCRIT          0.099000    0.148000    0.200000    0.255000
0.311000
```

```
                0.368000    0.465700    0.569400    0.690100
0.964800
*MW             16.04300    30.07000    44.09700    58.12400
72.15100
                86.17800   114.43000   144.83000   177.78000
253.63000
*VSHIFT        -0.217010    0.000000    0.000000    0.000000
0.000000
                0.000000    0.258450    0.205220    0.164540
0.094711
*BIN
     0.0
     0.0         0.0
     0.0         0.0         0.0
     0.0         0.0         0.0         0.0
     0.0         0.0         0.0         0.0         0.0
     0.0         0.0         0.0         0.0         0.0         0.0
        0.0
     0.0         0.0         0.0         0.0         0.0         0.0
        0.0         0.0
     0.2466      0.0         0.0         0.0         0.0         0.0
        0.0         0.0         0.0
*PHASEID      *GAS
*PSAT         3500.
*RHOW         1587.757
*CW           3.6E-06
*REFPW        3550.
*VISW         0.3049


RESULTS SECTION MODELARRAYS
RESULTS SECTION ROCKFLUID
**-------------------------------------------------ROCK FLUID---------
-

*ROCKFLUID


*RPT 1  *DRAINAGE
*SWT
0.160000  0.000000  0.740000  50.000000
0.200000  0.002000  0.680000  32.000000
0.240000  0.010000  0.620000  21.000000
0.280000  0.020000  0.562000  15.500000
0.320000  0.033000  0.505000  12.000000
0.360000  0.049000  0.450000  9.200000
0.400000  0.066000  0.400000  7.000000
0.440000  0.090000  0.348000  5.300000
0.480000  0.119000  0.300000  4.200000
0.520000  0.150000  0.260000  3.400000
0.560000  0.186000  0.222000  2.700000
0.600000  0.227000  0.187000  2.100000
0.640000  0.277000  0.156000  1.700000
0.680000  0.330000  0.126000  1.300000
0.720000  0.390000  0.100000  1.000000
0.760000  0.462000  0.078000  0.700000
```

```
0.800000  0.540000  0.058000  0.500000
0.840000  0.620000  0.040000  0.400000
0.880000  0.710000  0.026000  0.300000
0.920000  0.800000  0.013000  0.200000
0.960000  0.900000  0.005000  0.100000
0.995000  1.000000  0.000000  0.000000

*SGT
0.005000  0.000000  0.740000  0.000000
0.040000  0.005000  0.650000  0.000000
0.080000  0.013000  0.513000  0.000000
0.120000  0.026000  0.400000  0.000000
0.160000  0.040000  0.315000  0.000000
0.200000  0.058000  0.250000  0.000000
0.240000  0.078000  0.196000  0.000000
0.280000  0.100000  0.150000  0.000000
0.320000  0.126000  0.112000  0.000000
0.360000  0.156000  0.082000  0.000000
0.400000  0.187000  0.060000  0.000000
0.440000  0.222000  0.040000  0.000000
0.480000  0.260000  0.024000  0.000000
0.520000  0.300000  0.012000  0.000000
0.560000  0.348000  0.005000  0.000000
0.600000  0.400000  0.000000  0.000000
0.640000  0.450000  0.000000  0.000000
0.680000  0.505000  0.000000  0.000000
0.720000  0.562000  0.000000  0.000000
0.760000  0.620000  0.000000  0.000000
0.800000  0.680000  0.000000  0.000000
0.840000  0.740000  0.000000  0.000000

*KROIL *STONE2 *SWSG


RESULTS SECTION ROCKARRAYS
RESULTS SECTION INIT
**-----------------------------------------------------INITIAL CONDITION--
-
*INITIAL
*VERTICAL *BLOCK_CENTER *COMP
*NREGIONS 1
*REFDEPTH   7400.
*REFPRES    3550.
*DWOC       7500.
*ZDEPTH
      7500. 0.6793 0.099 0.0591 0.0517 0.0269 0.0181 0.0399 0.0122
0.008 0.0058
*SEPARATOR
   815         80
   65          80
   14.7        60


RESULTS SECTION INITARRAYS
RESULTS SECTION NUMERICAL
**-------------------------------------------------NUMERICAL----------
-
```

```
*NUMERICAL
*NORM *PRESS 145.04
*NORM *GMOLAR 0.15
*NORM *SATUR 0.15

RESULTS SECTION NUMARRAYS
RESULTS SECTION GBKEYWORDS
RUN



DATE 1986 01 01

DTWELL 5.

AIMWELL WELLNN

*DTMAX 100.

*DTMIN 0.1

WELL  1 'PROD'
CYCLPROD 'PROD'
OPERATE MAX STG  6.2E+06 CONT
OPERATE MIN BHP  500. CONT

GEOMETRY K 1. 0.34 1. 0.
PERF GEO   'PROD'
      7 3 2 1.
      7 3 1 1.


WELL  2 'INJ'
INJECTOR 'INJ'
INCOMP CYCLING
OPERATE MAX STG  4.7E+06 CONT
OPERATE MAX BHP  4000. CONT

GEOMETRY K 1. 0.34 1. 0.
PERF GEO   'INJ'
      1 9 4 1.
      1 9 3 1.


TIME 365

TIME 730

TIME 1095

TIME 3652

SHUTIN 'INJ'

TIME 5478
```

```
STOP
**************************** TERMINATE SIMULATION
****************************

RESULTS SECTION WELLDATA
RESULTS SECTION PERFS
```

APPENDIX E

1-D LINEAR MODEL
(SPE3 COMPARATIVE SOLUTION PROJECT MODIFIED)

```
RESULTS SIMULATOR GEM
RESULTS SECTION INOUT

*TITLE1  'SPE3 modified to specify drawdown'
*INUNIT *FIELD

*INTERRUPT *INTERACTIVE
*RANGECHECK *ON
*XDR *ON
*MAXERROR  20
*WRST *TIME
*WPRN *WELL  *TIME
*WPRN *GRID  *TIME
*WPRN *ITER  *BRIEF
*WSRF *WELL 1
*WSRF *GRID 10
*DIARY *CHANGES
*OUTPRN *WELL *ALL
*OUTPRN *GRID ADS 'C1' SG SO PRES SW

*OUTPRN *RES *ALL
*OUTSRF *WELL     *PAVG
                  *PRES 2 1 1
                  *SO 2 1 1
                  *SG 2 1 1
                  *SW 2 1 1
                  *KRO 2 1 1
                  *KRG 2 1 1
                  *KRW 2 1 1
                  *PRES 40 1 1
                  *SO 40 1 1
                  *SG 40 1 1
                  *SW 40 1 1
                  *KRO 40 1 1
                  *KRG 40 1 1
                  *KRW 40 1 1

*OUTSRF *GRID PRES SO SG SW RHOO RHOG SIG VISO

*OUTSRF *RES *ALL
*DIM *MDDD 3000  **$ ModelBuilder passed through this Keyword




RESULTS XOFFSET 0.
RESULTS YOFFSET 0.
RESULTS ROTATION 0
```

```
GRID VARI 40 1 1
KDIR DOWN
DI IVAR
       1. 1.127 1.27 1.432 1.613 1.818 2.05 2.31 2.603 2.934 3.307
3.727 4.2 4.734
       5.336 6.013 6.777 7.639 8.609 9.703 10.935 12.325 13.89 15.655
17.644 19.886
       22.412 25.26 28.469 32.086 36.162 40.756 45.934 51.77 58.347
65.76 74.114
       83.53 94.142 106.103

DJ CON 933.381

DK CON 50.
PAYDEPTH ALL
       40*5025.




**$ RESULTS PROP NULL  Units: Dimensionless
**$ RESULTS PROP Minimum Value: 1  Maximum Value: 1
**$ 0 = NULL block, 1 = Active block
NULL CON 1.

**$ RESULTS PROP PINCHOUTARRAY  Units: Dimensionless
**$ RESULTS PROP Minimum Value: 1  Maximum Value: 1
**$ 0 = PINCHED block, 1 = Active block
PINCHOUTARRAY CON 1.
RESULTS SECTION GRID

RESULTS SPEC 'Grid Top'
RESULTS SPEC SPECNOTCALCVAL 0
RESULTS SPEC REGION 'All Layers (Whole Grid)'
RESULTS SPEC REGIONTYPE 0
RESULTS SPEC LAYERNUMB 0
RESULTS SPEC PORTYPE 1
RESULTS SPEC CON 5000
RESULTS SPEC STOP

RESULTS SPEC 'Grid Thickness'
RESULTS SPEC SPECNOTCALCVAL 0
RESULTS SPEC REGION 'Layer 1 - Whole layer'
RESULTS SPEC REGIONTYPE 1
RESULTS SPEC LAYERNUMB 1
RESULTS SPEC PORTYPE 1
RESULTS SPEC CON 50
RESULTS SPEC STOP
RESULTS PINCHOUT-VAL       0.0002 'ft'
RESULTS SECTION NETPAY
RESULTS SECTION NETGROSS
RESULTS SECTION POR

RESULTS SPEC 'Porosity'
RESULTS SPEC SPECNOTCALCVAL 0
```

```
RESULTS SPEC REGION 'Layer 1 - Whole layer'
RESULTS SPEC REGIONTYPE 1
RESULTS SPEC LAYERNUMB 1
RESULTS SPEC PORTYPE 1
RESULTS SPEC CON 0.13
RESULTS SPEC STOP

**$ RESULTS PROP POR  Units: Dimensionless
**$ RESULTS PROP Minimum Value: 0.065  Maximum Value: 0.13
POR IVAR
       0.065 38*0.13 0.065

RESULTS SECTION PERMS

**$ RESULTS PROP PERMI  Units: md
**$ RESULTS PROP Minimum Value: 0.15  Maximum Value: 15
PERMI IVAR
       15. 39*0.15


**$ RESULTS PROP PERMJ  Units: md
**$ RESULTS PROP Minimum Value: 0.15  Maximum Value: 15
PERMJ EQUALSI

**$ RESULTS PROP PERMK  Units: md
**$ RESULTS PROP Minimum Value: 0.015  Maximum Value: 1.5
PERMK EQUALSI * 0.1
RESULTS SECTION TRANS
RESULTS SECTION FRACS
RESULTS SECTION GRIDNONARRAYS
CPOR  MATRIX   4.E-06
PRPOR MATRIX   3900.

RESULTS SECTION VOLMOD
RESULTS SECTION SECTORLEASE

RESULTS SECTION ROCKCOMPACTION
RESULTS SECTION GRIDOTHER
RESULTS SECTION MODEL
*MODEL        *PR
*NC           10  10
*COMPNAME     'C1'        'C2'        'C3'        'C4'        'C5'
              'C6'        'C7-9'      'C10-11'    'C12-14'    'C15+'
*HCFLAG       0           0           0           0           0
              0           0           0           0           0
*TRES         200.
*PCRIT         40.000000   48.200000   42.010000   37.470000
33.310000
               29.920000   26.253000   23.184000   19.987000
12.554400
*TCRIT         194.44600   305.43000   369.90000   425.20000
469.60000
               507.90000   573.45000   637.79000   685.75000
748.33100
*AC             0.013000    0.098600    0.152400    0.201000
0.253900
```

```
                0.300700    0.361300    0.450100    0.533900
0.724400
*VCRIT          0.099000    0.148000    0.200000    0.255000
0.311000
                0.368000    0.465700    0.569400    0.690100
0.964800
*MW             16.04300    30.07000    44.09700    58.12400
72.15100
                86.17800   114.43000   144.83000   177.78000
253.63000
*VSHIFT        -0.217010    0.000000    0.000000    0.000000
0.000000
                0.000000    0.258450    0.205220    0.164540
0.094711
*BIN
     0.0
     0.0         0.0
     0.0         0.0         0.0
     0.0         0.0         0.0         0.0
     0.0         0.0         0.0         0.0         0.0
     0.0         0.0         0.0         0.0         0.0         0.0
     0.0         0.0         0.0         0.0         0.0         0.0
        0.0
     0.0         0.0         0.0         0.0         0.0         0.0
        0.0         0.0
     0.2466      0.0         0.0         0.0         0.0         0.0
        0.0         0.0         0.0
*PHASEID      *GAS
*PSAT         3500.
*RHOW         1587.757
*CW           3.6E-06
*REFPW        3900.
*VISW         0.3049


RESULTS SECTION MODELARRAYS
RESULTS SECTION ROCKFLUID
**----------------------------------------------------ROCK FLUID---------
-

*ROCKFLUID


*RPT 1  *DRAINAGE
*SWT
0.160000  0.000000  0.740000  50.000000
0.200000  0.002000  0.680000  32.000000
0.240000  0.010000  0.620000  21.000000
0.280000  0.020000  0.562000  15.500000
0.320000  0.033000  0.505000  12.000000
0.360000  0.049000  0.450000  9.200000
0.400000  0.066000  0.400000  7.000000
0.440000  0.090000  0.348000  5.300000
0.480000  0.119000  0.300000  4.200000
0.520000  0.150000  0.260000  3.400000
0.560000  0.186000  0.222000  2.700000
0.600000  0.227000  0.187000  2.100000
```

```
0.640000  0.277000  0.156000  1.700000
0.680000  0.330000  0.126000  1.300000
0.720000  0.390000  0.100000  1.000000
0.760000  0.462000  0.078000  0.700000
0.800000  0.540000  0.058000  0.500000
0.840000  0.620000  0.040000  0.400000
0.880000  0.710000  0.026000  0.300000
0.920000  0.800000  0.013000  0.200000
0.960000  0.900000  0.005000  0.100000
0.995000  1.000000  0.000000  0.000000

*SGT
0.005000  0.000000  0.740000  0.000000
0.040000  0.005000  0.650000  0.000000
0.080000  0.013000  0.513000  0.000000
0.120000  0.026000  0.400000  0.000000
0.160000  0.040000  0.315000  0.000000
0.200000  0.058000  0.250000  0.000000
0.240000  0.078000  0.196000  0.000000
0.280000  0.100000  0.150000  0.000000
0.320000  0.126000  0.112000  0.000000
0.360000  0.156000  0.082000  0.000000
0.400000  0.187000  0.060000  0.000000
0.440000  0.222000  0.040000  0.000000
0.480000  0.260000  0.024000  0.000000
0.520000  0.300000  0.012000  0.000000
0.560000  0.348000  0.005000  0.000000
0.600000  0.400000  0.000000  0.000000
0.640000  0.450000  0.000000  0.000000
0.680000  0.505000  0.000000  0.000000
0.720000  0.562000  0.000000  0.000000
0.760000  0.620000  0.000000  0.000000
0.800000  0.680000  0.000000  0.000000
0.840000  0.740000  0.000000  0.000000

*KROIL *STONE2 *SWSG


RESULTS SECTION ROCKARRAYS

**$ RESULTS PROP ADGMAXC 'C1'  Units: gmole/lb
**$ RESULTS PROP Minimum Value: 0.084843  Maximum Value: 0.084843
ADGMAXC 'C1' CON 0.084843

**$ RESULTS PROP ADGCSTC 'C1'  Units: 1/psi
**$ RESULTS PROP Minimum Value: 0.0008882  Maximum Value: 0.0008882
ADGCSTC 'C1' CON 0.0008882
RESULTS SECTION INIT
**-----------------------------------------------------INITIAL CONDITION--
-
*INITIAL
*VERTICAL *BLOCK_CENTER *COMP
*NREGIONS 1
*REFDEPTH   5000.
*REFPRES    3900.
*DWOC       7500.
*ZDEPTH
```

```
      7500. 0.6793 0.099 0.0591 0.0517 0.0269 0.0181 0.0399 0.0122
0.008 0.0058
*SEPARATOR
   815         80
   65          80
   14.7        60


RESULTS SECTION INITARRAYS
RESULTS SECTION NUMERICAL
**-----------------------------------------------------NUMERICAL----------
-
*NUMERICAL
*NORM *PRESS 145.04
*NORM *GMOLAR 0.15
*NORM *SATUR 0.15

RESULTS SECTION NUMARRAYS
RESULTS SECTION GBKEYWORDS
RUN



DATE 1986 01 01

DTWELL 5.

AIMWELL WELLNN

*DTMAX 10.

*DTMIN 0.001


**$ RESULTS PROP AIMSET  Units: Dimensionless
**$ RESULTS PROP Minimum Value: 1  Maximum Value: 1
AIMSET CON 1.

WELL  1 'PROD'
CYCLPROD 'PROD'
OPERATE MIN BHP  2000. CONT

GEOMETRY K 0.25 0.37 1. 1.39
PERF GEO   'PROD'
      1 1 1 1. OPEN FLOW-TO 'SURFACE'


WELL  2 'INJ'
INJECTOR 'INJ'
INCOMP SOLVENT  0.69101 0.097764 0.057928 0.050256 0.025929 0.017292
0.037386 0.011106 0.007062 0.004267
OPERATE MAX BHP  3910. CONT

GEOMETRY K 0.25 0.37 20000. 0.
PERF GEO   'INJ'
      40 1 1 1. OPEN FLOW-FROM 'SURFACE'
```

```
OPEN 'INJ'

DATE 1986 01 02

.
.
.

DATE 1986 12 31

TIME 365

TIME 730

TIME 1095

TIME 3652

OPEN 'INJ'

TIME 5478


STOP
***************************** TERMINATE SIMULATION
*****************************

RESULTS SECTION WELLDATA
RESULTS SECTION PERFS
```

VITA

Name:	Adedeji Ayoola Adeyeye
Permanent Address:	1412 Kingsgate Street, Mitchville, MD 20721.
E-mail:	dejiyeye@hotmail.com aaa1789@tamu.edu
Education:	(2000) B. S., Chemical Engineering, University of Lagos, Akoka-Yaba, Lagos, Nigeria. (2003) M.S., Petroleum Engineering, Texas A&M University, College Station, TX 77843-3116.